SIMULATION OF PHASE SPACE HOLE GROWTH AND THE DEVELOPMENT OF INTERMITTENT PLASMA TURBULENCE

Robert H. Berman, David J. Tetreault and

Thomas H. Dupree

PFC/JA-84-5

PACS: 52.25Gj, 52.35Ra, 52.65. + z

Abstract

An unstable, highly intermittent state of turbulence is observed to evolve from a quiescent homogeneous plasma that is linearly stable. This intermittent state, which consists of isolated phase space density holes, produces a pronounced non-Gaussian distribution of fluctuation amplitudes. The skewness becomes increasingly more negative with time. The plasma is nonlinearly unstable because the holes grow in amplitude by accelerating to regions of higher average phase space density. The instability can be interpreted as a collection of colliding, growing holes and, in its early stages, is consistent with theoretical predictions for the clump instability. A series of runs with a single isolated hole indicates that an isolated hole grows for any finite electron-ion drift velocity. The isolated hole growth rate is consistent with theoretical predicitions. The implications of the instability to laboratory and space plasma are discussed.

I. Introduction

We report here on a series of computer simulations that were designed to investigate localized non-wave-like phase space density fluctuations in plasma. Such fluctuations – called "clumps" [1] – have been shown to be an important component of the turbulence observed in recent computer simulations. For example, it was observed in the one species simulations of Ref. 2 that the decay of plasma fluctuations from a variety of initial conditions tends to produce clump fluctuations. Such clumps can be either depletions (holes; $\delta f \leq 0$) or enhancements ($\delta f \geq 0$) in the phase space density. Here, $\delta f = f - f_0$, where f is the phase space density and $f_0 = \langle f \rangle$ where $\langle \ldots \rangle$ denotes a spatial average. A depletion or hole in the phase space density tends to self-bind and, when in isolation, forms the trapped particle phase space eddy of a Bernstein-Greene-Kruskal (BGK) equilibrium. Enhanced phase space material self-repels and fills the interstitial phase space regions between the holes. In the related work of Ref. 3, it was shown that the mean square fluctuation amplitude due to clumps can increase with time in a two-species plasma, *i.e.*, clumps can be unstable. The condition for clump instability can be much less restrictive than that required for linear instability of waves. In particular, the simulations of Ref. 3 show that the clump instability in a one dimensional, ion-electron plasma with electron drift can occur for electron drift velocities significantly below that required for the linear ion-acoustic instability. We pursue these two investigations further here by probing the dynamics of isolated holes and the relationship of holes to the clump instability.

The simulation experiments can be divided into three classes depending on the initial conditions used. In one class of runs (random starts), we simulated an initially quiescent plasma. The initial electrostatic energy was near the thermal level and was due only to a random distribution of discrete particles. No macroscopic or collective fluctuations were present initially. Spatially homogeneous ion and drifting electron Maxwellian velocity distribution functions were set up initially. In the second class of runs (enhanced starts), the

initial ion fluctuation level was enhanced above the thermal level. This was acomplished by redistributing ions in phase space so that the phase space was filled with a "checkerboard" pattern of closely packed ion phase space holes (of the same depth) and, in order to conserve charge, an equal number of charge enhancements between the holes. In the third class (isolated hole runs), a single isolated phase space density hole was introduced initially into the ion distribution function which was otherwise a spatially homogeneous Maxwellian (the initial electron distribution function was also Maxwellian). Discrete particle fluctuations were suppressed initially by judicious rearrangement of the discrete particles (a so-called "quiet start"). Detailed phase space diagnostics were used to determine: (1) the emergence of isolated phase space holes from homogeneous background turbulence; (2) the probability distribution of fluctuation amplitudes $P(\delta f)$; (3) the growth rate of isolated holes and its dependence on electron drift velocity; and (4) the effect of discrete particle collisions (thermal fluctuations) on hole growth.

The principal results – discussed at length in Sec. IVa and Sec. IVb – can be summarized as follows

A. For random start runs, an instability occurs for electron drift velocities $v_D \gtrsim 1.5 v_{th,i}$, *i.e.*, significantly below the linear stability boundary of $v_D = 3.92 v_{th,i}$ for the simulation parameters used ($v_{th,i}$ is the ion thermal velocity). This onset of instability from thermal fluctuations for small but finite drift velocity is consistent with theoretical predictions[4,5]. In the early stage of the instability, the distribution of fluctuation amplitudes is nearly Gaussian and the growth of the instability is consistent with theoretical predicitions for the clump instability[5].

B. As the instability further evolves in the random start runs, isolated phase space density holes emerge and – except for infrequent encounters with other holes – tend

to persist and coexist with the smaller velocity scale background turbulence described in (A). The relative isolation or concentration of the holes in a small fraction of the available phase space – a feature we refer to as hole intermittency – appears to be a natural consequence of the turbulence. Once produced, the holes tend to grow in depth [see (E) below] by accelerating to regions of higher average phase space density. This intermittency and growth of the holes causes the distribution of fluctuation amplitudes to become non-Gaussian with the skewness becoming more negative with time. This is inconsistent with the Gaussian or near Gaussian distribution assumed by many analytical theories of plasma turbulence.

C. The results of the "enhanced start" runs were similar to those of the random start runs. Instability occurred for electron-ion drift velocities $v_D \geq 1.5 v_{th,i}$ as in (A) and hole intermittency developed as in (B).

D. Discrete particle collisions (thermal fluctuations) tend to destroy the small scale velocity structure of holes and contribute to the finite marginal point observed in the random start runs [see (A)]. We have estimated this collisional decay rate by measuring the effect of discrete particle collisions on the growth rate of an isolated hole. We adopt a simplified model[4] for the hole growth rate in the presence of discrete particle collisions: $\gamma = \gamma_h + \gamma_d$ where $\gamma_d = -D/\Delta v^2$ and γ_h is the isolated hole growth rate when $\gamma_d = 0$. Here D is the velocity space diffusion coefficient due to discrete particle fluctuations and Δv is the velocity width of the hole. Simulation results support this model and indicate that the marginal point observed in (A), and Ref 3, is due more to hole-hole collisions than to discrete particle collisions.

E. In the single isolated hole experiments, hole growth or instability was stu died in

detail. Hole growth occurs in regions of velocity space where the electron and ion average velocity gradients are nonzero and opposing. We find that the isolated hole instability is due to a simultaneous increase in both the hole velocity width and depth as the hole accelerates to a region of higher average phase space density. In contrast to a linearly unstable ion-acoustic wave, we observed *isolated* hole acceleration and growth in a drifting ion-electron plasma for finite values of the electron drift velocity well below the threshold value ($1.5v_{th,i}$) observed in (A). Apparently, an isolated hole will grow for arbitrarily small nonzero drifts.

The observed isolated hole growth rate is consistent with recent theoretical predictions[4]. In the theory, acceleration of an ion hole, for example, results from momentum exchange with resonant electrons that are reflected by the hole. If the velocity gradient of the average electron distribution function is positive ($\partial f_{0e}(v)/\partial v \geq 0$) at the velocity of the hole, the hole absorbs net momentum and decelerates to regions of higher f_{0i}. The hole depth thereby increases since f_i inside the hole must remain constant. The hole depth and velocity width increase simultaneously, since these quantities are related to each other through the hole self-binding (trapping) condition.

F. The simulation results (A) – (E) are consistent with a model that describes the unstable turbulence of the random and enhanced start runs as a collection of colliding, growing phase space density holes[2--5]. If we denote the fractional phase space area occupied by holes as p (the hole "packing fraction"), then the turbulence is composed of a $p \ll \frac{1}{2}$ distribution of intermittent, isolated holes emerging from a $p \approx \frac{1}{2}$ background of smaller velocity scale hole fluctuations. The instability observed is due to the production of new holes that result from the turbulent mixing of the average phase space density and to the acceleration of the emerging holes. Hole intermittency can develop and persist because an emerging hole can grow larger in amplitude than

its neighbors. This growth makes the hole increasingly less susceptible to decay by collisions with other holes.

The finite threshold drift required for instability in the enhanced runs (C) can be explained by the fact the collisions between holes lead to their decay. In the enhanced start runs, the onset of the instability occurs when the holes are densely packed (the hole packing fraction is one half) and, therefore, collisions between holes are frequent. Thus, instability can only occur when the growth rate of the holes exceeds their destruction rate due to hole-hole collisions. When the packing fraction is one half, the balance between these two competing rates occurs at a threshold drift of $v_D = 1.5 v_{th,i}$[2,5]. Note that in the case of an isolated hole (E), hole-hole collisions are absent and any finite drift velocity will lead to instability.

Collisions between holes can also explain the result that the enhanced and random start runs become unstable at the same threshold drift. In this regard, it is useful to think of the thermal fluctuations as a collection of holes. Discrete particle collisions can then be described as collisions between these "thermal holes"[4]. Recall that the onset of instability for the random start runs (A) occurred when the distribution of fluctuation amplitude, $P(\delta f)$, was nearly Gaussian. For holes with depths equal to the average thermal hole depth, the packing fraction is equal to one half so that the balance between growth and decay for these holes occurs at the threshold of $v_D = 1.5 v_{th,i}$. Note that the holes with depths greater than the average thermal depth have $p \leq \frac{1}{2}$ and therefore would grow at a lower threshold drift. However, such holes are exponentially smaller in number[4] so that instability occurs close to the $p = \frac{1}{2}$ threshold of $v_D = 1.5 v_{th,i}$.

These results depict a turbulent plasma that is fundamentally different than the traditional concept of waves and their linear instabilities. The results imply that instability can occur in plasma arbitrarily close to thermal equilibrium – one only needs a sufficiently small hole

packing fraction. As we will discuss in Sec. VI, this conclusion is of practical interest to both space and laboratory plasma since hole-clump instability can occur in plasma heretofore considered stable to linear ion acoustic waves. For example, though ion-acoustic waves are believed stable in current driven plasma where electron and ion temperatures are comparable and the current is small, holes and clumps can be unstable in such plasma. In addition, the hole-clump instability is consistent with the observations of double layers (holes) along auroral field lines[6] and may be relevant to anomalous reconnection processes in magnetic field reversed configurations such as the earth's magnetotail.

II. Theoretical Review

As discusssed in the Introduction, clump fluctuations can be either depletions (holes) or enhancements in the phase space density. Since a hole self-binds while a phase space enhancement self-repels, the holes play a central role in the nonlinear evolution of the plasma. This is particularly true when the hole packing fraction is small. Then, the plasma can be viewed as a collection of infrequently interacting, approximate BGK equilibria. However, when the packing fraction is nearly one half, frequent collisions between holes significantly destroy individual hole equilibria and identity. The turbulence is then more appropriately described as small granulations (both positive and negative) in the phase space density. We refer to these small velocity scale fluctuations as clumps.

The origin of a clump fluctuation can be traced to the mixing of the phase space density by turbulent electric fields in a Vlasov plasma[1,7]. Because the Vlasov equation preserves phase space density along particle orbits, regions of different density cannot interpenetrate (the flow is incompressible). Any mixing of the phase space density will, therefore, be imperfect and lead to a graininess of the distribution function. Such a phase space density granulation or clump is a group of particles, all moving at approximately the same speed. This macroparticle will tend to be destroyed by the velocity dispersion of its constituent

particles and by "collisions" with other fluctuations in the plasma. As a result, neighboring particles in a clump will undergo stochastic instability. The neighboring orbits will deviate from each other exponentially in time – the characteristic time for separation being referred to as the Liapanov time or clump lifetime. In this simplified stochastic instability model of clumps, the mean square fluctuation level decays on the Liapanov time scale. However, as observed in the simulation described in Ref. 2, neighboring particle orbits undergo stochastic instability, but the mean square fluctuation level decays at a slower rate than the Liapanov rate. The reason for this discrepancy lies in the self-binding feature of the holes. Although holes tend to collide and fragment (on the Liapanov time scale), the hole fragments tend to recombine into new hole fluctuations. The recombination tendency of the holes is not an individual orbit modification and, therefore, is not described by the usual stochastic instability model. At present, there is no analytical theory of clump decay which includes hole self-binding. However, a phenomenological model has been developed that is consistent with the computer simulations described in Refs. 2 and 3.

An important feature of clump fluctuations is their ability to regenerate themselves and grow in amplitude (become unstable)[1,8]. Though velocity dispersion and diffusion tend to destroy a clump once it is produced, the turbulent electric fields simultaneously create new clumps by mixing the phase space density. Moreover, existing clumps tend to accelerate to regions of larger phase space density and thereby grow in amplitude. Plasma will be unstable to clumps when these production rates exceed the clump destruction rate. This "clump instability" occurs for a finite electron drift velocity in a drifting ion-electron plasma and has been observed in the computer simulations of Ref. 3 and in the numerical solution of clump model equations[8]. The clump model assumes that $p \approx \frac{1}{2}$ and therefore describes clump turbulence by the two-particle fluctuation correlation function $\langle \delta f(x_1, v_1, t) \delta f(x_2, v_2, t) \rangle$. The model equations are of the form

$$\left(\frac{\partial}{\partial t} + T_{12} \right) \langle \delta f(1) \delta f(2) \rangle = S_{12} \tag{1}$$

where the source term S_{12} describes clump acceleration and the mixing of the average

phase space density. The T_{12} term describes clump decay. The finite electron drift velocity required for clump instability is therefore due to the competition between the T_{12} and S_{12} terms in Eq. (1). In the simplest case where the particles are ballistically streaming and diffusing in velocity space, neighboring particle orbits undergo stochastic instability. Then, clump fluctuations decay at the rate $T_{12} \approx \tau_{cl}^{-1}(x_-, v_-)$ where $\tau_{cl}(x_-, v_-)$, given by Eq. (48), is the characteristic time for two orbits (separated initially by $x_- = x_1 - x_2$, $v_- = v_1 - v_2$) to remain correlated. However, the simulations of Ref. 2 suggest that the self-binding of the hole fluctuations reduces the decay rate to $T_{12} \approx (b\tau_{cl})^{-1}$ where $b \approx 3$. With this simplified model of hole self-binding, the calculations of Ref. 5 show that the clump growth rate derived from Eq. (1) agrees well with the growth rate observed in the simulations of Ref. 3 where p remained approximately one half during the measurements.

Another important feature of clump fluctuations is not (and probably cannot be) described by a model equation such as Eq. (1). As discussed in Ref. 2, decaying turbulence [corresponding to $S_{12} = 0$ in Eq. (1)] evolves into a highly intermittent state consisting of isolated phase space holes. The mean square fluctuation level $\langle \delta f^2 \rangle$ decays as the phase space area occupied by the holes decreases with time, *i.e.*, the hole packing fraction p decreases with time. This characteristic of decaying turbulence is outside the scope of Eq. (1) which assumes that fluctuations are closely packed in phase space, *i.e.*, p is close to one-half. A related difficulty with Eq. (1) is that the two-point fluctuation correlation function cannot distinguish between positive fluctuations ($\delta f \geq 0$ which self-repel) and negative fluctuations ($\delta f \leq 0$ which self-bind). In the highly intermittent state where $p \ll 1$, regions where $\delta f \geq 0$ will have a very much smaller $|\delta f|$ than regions where $\delta f \leq 0$. As reported in Ref. 2, such a state of hole intermittency with $p \ll 1$ has a pronounced non-Gaussian distribution of fluctuation amplitudes $P(\delta f)$. There, $P(\delta f)$ is significantly skewed towards $\delta f \leq 0$. Moreover, the skewness increases with time as the turbulence decays and p decreases.

Equation (1) similarly fails in describing the unstable, intermittent turbulence discussed

in Sec. IV. There, we report that a highly intermittent state of hole turbulence evolves from an unstable plasma characterized initially by $p \approx \frac{1}{2}$ turbulence and a $I'(\delta f)$ that is Gaussian. The hole intermittency occurs for both nonlinearly (clump) unstable and linearly unstable plasma. In both cases, isolated holes emerge from the $p \approx \frac{1}{2}$ background and $I'(\delta f)$ becomes strongly non-Gaussian. The plasma is therefore driven from a $p \approx \frac{1}{2}$ state to one where $p \ll \frac{1}{2}$. However, the phase space mixing and diffusion terms in Eq. (1) tend to drive the plasma toward $p \approx \frac{1}{2}$ rather than toward $p \ll \frac{1}{2}$.

Although Eq. (1) applies only to the $p \approx \frac{1}{2}$ case, it nevertheless contains some of the features of the isolated hole instability. As discussed in Refs. 4 and 5, the clump instability can be viewed as the many-interacting hole analog of the isolated hole instability (see also Sec. V below). The difference between the two regimes lies in the effects of large and small hole packing fraction p. In the isolated hole instability, p approaches zero. Then, neglecting discrete particle collisions, an infinitesimal free energy source will lead to hole acceleration and growth. For example, an ion hole whose velocity u is such that $\partial f_{0e}(u)/\partial u \geq 0$ will absorb net momentum from reflecting electrons and thus, decelerate unimpeded to regions of higher phase space density. However, when p approaches $\frac{1}{2}$, as in the clump instability, collisions between holes lead to fluctuation decay and, hence, to a finite free energy threshold for instability (*i.e.*, collisions between holes impede hole acceleration). In this latter regime, hole-hole collisions also mix the phase space density and thereby produce new holes throughout the phase space. These features are represented in Eq. (1). The T_{12} term describes collisions between fluctuations while the source term S_{12} – composed of two terms – describes hole acceleration (growth) as well as the production of new holes by the mixing of the average phase space density. Therefore, neglecting discrete particle collisions, the clump instability described by Eq. (1) "reduces" to the isolated hole instability, since, as $p \to 0$, the fluctuation decay term $T_{12} \to 0$ and the source term S_{12} of the growing species contains only the contribution from hole acceleration. In this sense, the isolated hole instability and the clump instability are complementary regimes of the same

nonlinear instability.

III. Simulation Code and Diagnostics

For our simulations we used a highly optimized, one-dimensional electrostatic code with $N_p = 102400$ particles per species and a spatially periodic system of length $L = 10\pi\lambda_D$ (λ_D is the Debye length). Therefore, the number of particles per Debye length was $n_0\lambda_D = 3259.5$ ($n_0 = N_p/L$ is the spatial particle density). The electrons and ion trajectories were obtained by using a finite time step of $0.2\omega_{p_e}^{-1}$ (ω_{p_e} is the electron plasma frequency) and solving Poisson's equation on a grid divided into $N_g = 512$ zones. A spatial average over the length of the system is defined as

$$\langle F \rangle = \frac{1}{L}\int_0^L F\,dx. \tag{2}$$

Because small velocity scale fluctuations such as clumps are very easily destroyed by discrete particle collisions, we would have preferred to use as large a value of $n_0\lambda_D$ as possible. Given the constraints of limited computer resources, we chose the relatively large value of $n_0\lambda_D \approx 3300$. As we report in Sec. IVc, this value of $n_0\lambda_D$ did not cause significant disruption of the small scale velocity structure of the fluctuations. It is interesting to contrast this case with waves that have velocity structure on the order of v_{th} and are, therefore, less disrupted by discrete particle fluctuations. This suggests that high collisionality may be one reason that clump fluctuations have not been previously observed in the numerous computer simulations of the last twenty years. Because of our limited computer time and our use of large $n_0\lambda_D$, we were forced to use a low value of ion to electron mass ratio m_i/m_e. We chose $m_i/m_e = 4$ so that the shortest electron and ion response times would not be too disparate ($\omega_{p_e} = 2\omega_{p_i}$ for $m_i/m_e = 4$).

Our particular choices of parameters ensured that rapid quasi-linear plateauing of the particle distribution functions did not occur and thereby precipitously shut off the source of available free energy necessary for instability. The choice of low mass ratio and large $n_0\lambda_D$

resulted in a plateau rate due to discrete particle collisions that was much less than typical instability growth times. Use of a larger mass ratio would lead to a more narrow resonant velocity region in the elctron distribution function and therefore, to a more rapid plateauing rate. In addition, our choice of periodic system length L ensured (for our chosen mass ratio) that electrons reflected by an ion hole would not transverse the periodic system length before the hole could grow appreciably. If this were not the case, the electron distribution function would plateau in the resonant velocity region of the hole, thereby dissipating the free energy driving the hole growth.

As is convenient in particle-mesh simulations, we modified the interparticle force at short distances to better approximate a collisionless system. This was done by choosing finite-size particle shapes and interpolation schemes designed to satisfy various criteria, *e.g.*, conservation of momentum or energy, isotropy of force, accuracy at short distances, or to reduce the influence of unphysical, large wavenumbers[9]. These choices may be combined into a single "shape factor," S, which appears in the Fourier transform of Poisson's equation as $k^2\phi(k) = 4\pi S(k) \int dv\, \delta f(k)$. We have repeated a single isolated hole experiment with numerous shape factors that test each of these criteria and have found no significant physical differences in the growth rate of the hole or its evolution in phase space. We are confident that our physical results are independent of simulation technique.

For initial conditions, we used an unshifted Maxwellian velocity distribution function for the ions $\{f_{0i}(v) = (2\pi v_{th,i}^2)^{-1/2} \exp[-v^2/(2v_{th,i}^2)]\}$ while for the electrons we used a shifted Maxwellian with drift velocity v_D relative to the ions $\{f_{e0}(v) = (2\pi v_{th,e}^2)^{-1/2} \exp[-(v - v_D)^2/(2v_{th,e}^2)]\}$. At $v = 0$ in the ion distribution function, the average number of particles in a phase space cell of size $\Delta x_w = 1\lambda_D$ by $\Delta v_w = 0.1 v_{th,i}$ was $\langle N \rangle = 130.35$. The electrons had typical drift velocities in the range $0 \leq v_D \leq 4.2 v_{th,i}$. For "random starts", the particles were distributed randomly, but homogeneously, in space. The initial electrostatic energy was, therefore, close to the thermal (shielded discrete particle) level. Figure 2a shows the initial ion phase space typical of the random start. In the "quiet starts" discussed in

Sec. IVb, an ion hole was introduced initially, but all other initial fluctuations, *i.e.*, thermal fluctuations, were suppressed. This typically produced electrostatic energy levels some 10^{-7} of the thermal level. Thermalization from the quiet start generally took some $200\omega_{p_e}^{-1}$. The intitial ion phase space typical of the quiet start is shown in Fig. 8a.

We have found here and in previous work[2,3] that the conventional diagnostics used in simulations of plasma turbulence do not expose some important features of the turbulence. For example, phase space pictures have a strong intuitive appeal (and we include some of them here), but they do not reveal the detailed local structure and evolution of the fluctuations. The mean square electric field – another widely used diagnostic – is also insensitive to local phase space structure since the electric field $E(x, t)$ is a velocity integral over the distribution functions. A related problem is that plasma normal modes can easily be excited (*e.g.*, by initial conditions) and can dominate the mean square electric field. For example, long-lived electron plasma oscillations at phase speeds $v_{ph} \geq v_{th,e}$ can mask localized phase space fluctuations at phase speeds $v_{ph} \leq v_{th,e}$. The conventional electric field spectrum [$E^2(k)$ where k is the wavenumber] will not resolve these two distinct fluctuations since a resolution of *phase velocity* is required. We have therefore developed detailed phase space diagnostics that are sensitive to the *local* phase space properties of the fluctuations.

Specific diagnostics were devised to probe the phase space structure of an individual hole. We focused primarily on ion holes although runs with electron holes yielded analogous results. Initially, 1000 test or "marker" particles were distributed uniformly inside the phase space boundaries of the ion hole. The test particles did not contribute to Poisson's equation and did not affect the fields or forces in the system. The marker particles do not describe the full phase space width (Δx, Δv) of a hole but, to the extent that they remain grouped together, give information on time history of the hole. For example, if the hole accelerates, but remains as a trapped particle structure, the marker particles will remain trapped in the hole and will provide information on the hole motion. In particular, knowledge of the marker

particle positions allow an instantaneous measurement of the depth of an acclerating hole. We display the marker particles in some of the phase space pictures below. The motion of the marker particles is particularly evident in Figs. 5.

We performed a number of additional detailed phase space diagnostics every $10\omega_{p_e}^{-1}$. We divided the phase space into cells of size Δx_w by Δv_w and counted the number N of particles per cell. We then calculated the mean number of particles per cell $\langle N \rangle$ and the fluctuation about the mean, $\delta N = N - \langle N \rangle$. The particle distribution function, averaged over a cell is $\overline{f} = N/(\delta x \delta v)$ and the fluctuation is $\overline{\delta f} = \delta N/(\delta x \delta v)$. Here, we denote the average over a cell by the overline.

The measurements of the number fluctuation δN were used to calculate the probability distribution function $P(\overline{\delta f})$ of finding a fluctuation $\overline{\delta f} = \delta N/(\delta x \delta v)$ in a phase space cell of size δx by δv. The importance of $P(\overline{\delta f})$ lies in the fact that it contains information about both the sign and magnitude of the fluctuations. Any tendency of the turbulence to preferentially produce negative fluctuations in isolated regions of phase space will be readily apparent from the form of $P(\overline{\delta f})$. We also note that $P(\overline{\delta f})$ contains information about all the correlation functions, *i.e.*, the familiar two-point correlation function evaluated at zero phase space separation is given by $\int d\overline{\delta f}\, \overline{\delta f}^2 P(\overline{\delta f})$. Although the two-point correlation function is indifferent to the sign of $\overline{\delta f}$, the skewness s of $P(\overline{\delta f})$

$$s = \frac{\int d\overline{\delta f}\, \overline{\delta f}^3 P(\overline{\delta f})}{[\int d\overline{\delta f}\, \overline{\delta f}^2 P(\overline{\delta f})]^{3/2}} \tag{3}$$

can be used to probe negative fluctuations. We obtained $P(\overline{\delta f})$ by making a histogram of the δN measurements. Typical phase space window sizes varied between $\lambda_D \leq \Delta x_w \leq 3\lambda_D$ and $0.05 v_{th,i} \leq \Delta v_w \leq 0.3 v_{th,i}$.

Information on all the fluctuations in the plasma, *i.e.*, waves, clumps and discrete particle fluctuations, will be contained in δN and $P(\overline{\delta f})$. Unless we contrive the initial conditions (e.g., suppress *all* initial fluctuations with a "quiet start") discrete particle fluctuations will always be present. We can estimate their effects as follows. First, for discrete particles that

are randomly distributed in a cell, $\langle \delta N^2 \rangle = \langle N \rangle$. However, for fluctuations moving at phase speeds near the zeros of the plasma dielectric function, $\langle \delta N^2 \rangle$ will be enhanced through the emission and absorption of weakly damped waves. We have calculated this enhanced contribution to $\langle \delta N^2 \rangle$ and have found it to be, consistently, much smaller than the values of $\langle \delta N^2 \rangle$ observed during instability. Next, the effect of particle discreteness on $P(\overline{\delta f})$ can be estimated by considering $P(\overline{\delta f})_{th}$ where, in each cell, f is Gaussian with a mean value f_0:

$$P(\overline{\delta f})_{th} = [2\pi f_0^2/\langle N \rangle]^{-1/2} \exp\left[-\frac{\langle N \rangle}{2}\left(\frac{\overline{\delta f}}{f_0}\right)^2\right] \tag{4}$$

Therefore, the width of the discrete particle contribution to $P(\overline{\delta f})$ will be small for large $\langle N \rangle$, *i.e.*, cells with large Δx_w and Δv_w. This also implies that the smaller cells – where the contributions to $P(\overline{\delta f})$ will be due almost entirely to discrete particle fluctuations – will have a (nearly) Gaussian $P(\overline{\delta f})$. The $P(\overline{\delta f})$ measurements discussed in this paper are significantly broadened above the discrete particle level. We stress again the importance of this low discrete particle collisionaility in the simulations. Use of too few particles leads to the destruction of the clumps' small scale velocity structure.

IV. Simulation Results

a. Random Starts and the Development of Hole Intermittency

We made a series of runs with random starts (see Sec. III) and various electron drift velocities below the linear stability boundary of $3.9v_{th,i}$. We stress that no hole was introduced initially in the particular runs discussed in this Section IVa. Results for a representative run with $v_D = 3.5v_{th,i}$ are shown in Figs. 1 – 4. Figure 1 shows the electron and ion distribution functions at $\omega_{p_e}t = 0$ and at $\omega_{p_e}t = 260$. The initial ion phase space is shown in Fig. 2A. As reported in Ref. 3, such a plasma is nonlinearly unstable. Fluctuations develop and considerable distortion of the ion distribution function

and flattening of the electron distribution function take place (see Fig. 1). This plateauing of the electron distribution function appears to be the saturation mechanism of the instability. As discussed in Ref. 3, similar features have been observed for drift velocities in the range $1.5v_{th,i} \leq v_d \leq 4.5v_{th,i}$. This range contains drifts above and considerably below the linear stability boundary of $v_D = 3.9v_{th,i}$ for this problem.

The emergence of intermittent, macroscopic phase space holes from the near thermal noise of Fig. 2A can be seen from the time sequence of phase space pictures of Figs. 2B through 2X. Figure 2B is the ion phase space at $\omega_{p_e}t = 230$ while each subsequent figure is $10\omega_{p_e}^{-1}$ later than the preceding one (Figure 2X is at $\omega_{p_e}t = 450$). The y-axis is normalized ion velocity $v/v_{th,i}$ with divisions of 0.5. The velocity $v = 0$ is at the exact midpoint of the y-axis of the pictures. The x-axis is normalized position x/λ_D with divisions of 2.0.

Although holes are evident in any one of the pictures in Fig. 2, the more interesting observation is that of individual hole motion and persistence throughout the run. Therefore, a large number of pictures are presented in Fig. 2 in order to emphasize the time evolution of holes at the expense of illustrating more detailed structure at a fixed time. However, in spite of a smaller picture size, an indivdual hole can be identified and its motion can be followed in time from picture to picture. This can be done as follows. Once a hole is identified in a particular picture, its position in the next picture can be anticipated by knowing the hole velocity and the time interval $10\omega_{p_e}^{-1}$ between pictures. For example, the ion hole, which we denote H1, at phase space coordinates $(x, v) = (4\lambda_D, 0.25v_{th,i})$ in Fig. 2B can be traced through succeeding pictures to the coordinates $(x, v) = (31\lambda_D, -0.3v_{th,i})$ in Fig. 2I. Two other holes in Fig. 2B – H2 at $(3\lambda_D, v_{th,i})$, and H3 at $(2\lambda_D, 1.5v_{th,i})$ – can be traced forward to $(22\lambda_D, 0.5v_{th,i})$ and $(31\lambda_D, 0.75v_{th,i})$ in Fig. 2I. In this process, all three holes have emerged out of the homogeneous background shown in Fig. 2A. As holes H1, H2 and H3 evolve, additional new holes emerge at $(2\lambda_D, 1.2v_{th,i})$ in Fig. 2K, at $(5\lambda_D, 1.5v_{th,i})$ in Fig. 2P, and at $(5\lambda_D, v_{th,i})$ in Fig. 2R. These fluctuations are not wave-like, but are localized phase space density holes with scale lengths on the order of several

Debye lengths and velocity widths less than the thermal velocity.

Except for infrequent encounters (collisions) with other holes, the emerging holes tend to grow by decelerating to regions of larger phase space density. Consider holes H2 and H3 in Fig. 2B. As H3 decelerates to $(8\lambda_D, 0.6v_{th,i})$ in Fig. 2C, it collides with H2 (see Figs. 2C - 2F). The two holes subsequently decouple (see Figs. 2G and 2H) and each resumes its deceleration. The deceleration of H2 can be seen by noting its locations at $(22\lambda_D, 0.5v_{th,i})$ in Fig. 2I, $(25\lambda_D, 0.3v_{th,i})$ in Fig. 2K, $(26\lambda_D, 0)$ in Fig. 2M, $(23\lambda_D, -0.5v_{th,i})$ in Fig. 2O, $(13\lambda_D, -0.75v_{th,i})$ in Fig. 2R, $(29\lambda_D, -1.2v_{th,i})$ in Fig. 2U, and $(23\lambda_D, -1.4v_{th,i})$ in Fig. 2V. The hole velocity passes through zero in Fig. 2L. For hole velocities greater than zero, the hole velocity width Δv appears to increase with time, while for velocities less than zero, the width decreases. Alternate growth and decay of the hole occurs although the hole acceleration remains negative throughout the hole's motion. Similar behavior can be seen in the motion of hole H1 at $(4\lambda_D, 0.25v_{th,i})$ in Fig. 2B: its velocity passes through $v = 0$ at $\omega_{p_e}t = 240$ in Fig. 2C and through $v = -0.5v_{th,i}$ at $\omega_{p_e}t = 320$ in Fig. 2K. Hole H1 subsequently decays and disappears into the background turbulence.

We obtained quantitative measurements of the ion hole deceleration by measuring $P(\overline{\delta f})$ and its time dependent skewness $s(t, v)$ for various phase velocities $v/v_{th,i} = 0, 0.25, 0.5$ and 1.0 in the ion distribution. These are shown in Fig. 3 for a window of size $\Delta x_w = \lambda_D$ by $\Delta v_w = 0.1v_{th,i}$. Though $P(\overline{\delta f})$ is nearly Gaussian early in the run, significant negative skewness, *i.e.*, $s(t, v) \leq -1$, develops as the instability evolves ($|s|$ values of order of or less than 0.3 are statistical noise). The successive fall and rise of $s(t, v)$ in time for progressively smaller velocities v is evident from Fig. 3. The skewness $s(t, v)$ is most negative when a hole is at velocity v and time t. Therefore, a single decelerating hole will cause $s(t, v)$ to assume local minimum values for sucessively smaller velocities at increasing times. The local minimum values of $s(t, v)$ at $(t, v) = (180\omega_{p_e}^{-1}, 0.5v_{th,i})$, $(200\omega_{p_e}^{-1}, 0.25v_{th,i})$ and $(240\omega_{p_e}^{-1}, 0)$ (see Fig. 2C) correspond to the presence of hole H1 at these (t, v) values. Although $s(t, 0)$ increases after hole H1 passes, it decreases again as hole H2 approaches $v = 0$. For

example, hole H1 pass through $v = 0$ at $\omega_{p,e}t = 240$ (see Fig. 2C) while hole H2 pass through $v = 0$ at $\omega_{p,e}t = 330$ (see Fig. 2L). We also detected the presence of a single hole directly in $I'(\overline{\delta f})$ Figure 4a shows $I'(\overline{\delta f})$ at $v = 0$ before hole H1 has decelerated to $v = 0$ and Fig. 4b shows $I'(\overline{\delta f})$ when hole H1 is at $v = 0$. The presence of the hole H1 changes $I'(\overline{\delta f})$ from Gaussian to non-Gaussian.

Similar runs made with varying electron drifts down to a value of $v_D = 1.5v_{th,i}$ also show intermittent turbulence. This tendency of the turbulence to preferentially produce relatively isolated holes during the simulations is evident from the $s(t, v)$ curves of Fig. 3. When averaged over phase velocities v, the average skewness is negative throughout the run. The emergence of isolated holes from the background turbulence and their subsequent persistence and growth appear to be general features of the turbulence.

These features of hole intermittency and growth are characteristic of turbulence that evolves from a linearly unstable plasma as well. Figures 5 and 6 show electron and ion phase space holes which evolved in a random start run with a drift of $v_D = 4.2v_{th,i}$, *i.e.*, above the linear stability boundary of $v_D = 3.9v_{th,i}$. For the same elapsed time, the holes are much larger in depth and accelerate faster than those in the linearly stable case in Fig. 2 where $v_D = 3.5v_{th,i}$. This suggests that the hole growth rate increases with v_D (see Fig. 14). Figure 5 shows a time sequence of ion phase space pictures for this case where hole self-binding and acceleration are spectacularly demonstrated. Though no ion hole was initially introduced, ion marker particles were placed initially as shown in Fig. 5A. As the instability evolved, an ion hole emerged and trapped some of the ion marker particles. As is evident in Figs. 5B – 5J, the ion hole decelerated – carrying some of the ion marker particles along with it. The hole deceleration is considerably faster than that of the ion holes in Fig. 2 where v_D is smaller. The eddy-like phase space structure of the trapped marker particles is apparent as they oscillate in the ion hole potential. The trail of marker particles in the "wake" of the decelerating hole is also evident. These particles are disrupted and lost from the hole due to the background turbulence (both thermal and collective fluctuations). In

spite of these disruptions, the hole clearly grows and decelerates rapidly. The growth and subsequent decay of the hole velocity width as it moves from $v \geq 0$ to $v \leq 0$ is also clear.

The trapping or self-binding feature of the holes is evident in the tendency of holes to attract each other. Such tendencies to merge or coalesce can lead to "tidal" collisions as in Figs. 2B – 2H, or to the formation of a new hole. Figure 6 shows the formation of a new electron hole by the coalescing of two existing (parent) electron holes. The parent holes emerged spontaneously from the same linearly unstable, random start run that led to the ion hole depicted in Fig. 5. The coalescing of holes has also been observed in Ref. 11 and elsewhere. Apparently, hole coalescing tends to produce holes with progressively larger spatial scales[10]. A close examination of Figs. 2R – 2X also indicates that the plasma tends to produce holes with larger spatial scales. Figure 6 shows that the coalescing electron holes accelerate to a region of higher electron phase space density. The holes proceed deep into the electron distribution function because the ion tail (with negative slope) has been pulled out to these velocities by the turbulence (as in Fig. 1).

b. Isolated Hole Starts and Hole Growth

In order to further study the phase space hole growth observed in Sec. IVa, we made a series of quiet start runs with an isolated ion hole initially present. The runs discussed in this Section IVb all have an initial ion hole whose depth is $\tilde{f}/f_{0i} = -0.6$ and whose size is $\Delta x = 6\lambda_D$ by $\Delta v = 0.2v_{th,i}$. Holes with smaller $\tilde{f}$, Δx or Δv yielded similar results but were more difficult to study. For example, shallow holes were more difficult to see in the phase space pictures. In addition, holes smaller in Δv and $\tilde{f}$ have correspondingly lower growth rates. Consequently, such holes have a greater susceptibility to decay by discrete particle collisions and (for the same system length and mass ratio) may not grow before free energy is dissipated by quasilinear plateauing. The initial hole was prepared by "digging out" a rectangular shaped hole in the ion phase space and placing the particles thereby removed at random in a velocity strip of phase space that was centered at the hole velocity and had

the same width Δv as the hole. This strip of enhanced phase space density quickly streams apart in x and self-repels apart in v so as to disperse throughout a large portion of the phase space. Figure 8a shows the initial phase space density for a run with $v_D = 3.0 v_{th,i}$ and is typical of the initial conditions used in the isolated hole runs discussed in this Section IVb.

We made the initial $\tilde{f}$, Δx, Δv values of the ion hole reasonably close to an equilibrium BGK hole (see Sec. Va), but a precise equilibrium configuration was very difficult to prepare. In particular, we did not take into account Debye shielding of the hole and adjustment of the ion particles removed from the hole. Figure 7 shows a typical initial time sequence (with $20\omega_{p_e}^{-1}$ between Figures) where the initial rectangular hole equilibrates into a BGK mode characterized by $\Delta v \approx 0.6 v_{th,i}$ and $\Delta x \approx 5\lambda_D$. Equilibration occurs at approximately $50\omega_{p_e}^{-1}$, *i.e.*, a few trapping times. This time is considerably shorter than the time for the discrete particle fluctuations to rise to the thermal level. The initial distortions of the phase space hole are due to ion Landau damping and trapped particle oscillations in the hole as equilibration occurs (see Sec. Va).

A case of linearly stable drift ($v_D = 3.0 v_{th,i}$) is shown in Figs. 8 - 10. The initial conditions for this run are shown in Fig. 8A. The ion hole placed initially at $(10\lambda_D, 1.5 v_{th,i})$ in Fig. 8A, has evolved to $(22\lambda_D, 0.75 v_{th,i})$ at $\omega_{p_e} t = 120$ (see Fig. 8B). The deceleration process continues as the hole passes through $v = 0$ at $\omega_{p_e} t = 180$ (see Fig. 8G). The hole deceleration is also evident from the center marker velocity shown in Fig. 9. From Figs. 9 and 10, we note that the hole depth increases with time for positive hole velocities but decreases for negative hole velocities. Referring to Fig. 1, it is apparent that the hole depth grows in regions where $f'_{0e} f'_{0i} \leq 0$ but decays where $f'_{0e} f'_{0i} \geq 0$. The cessation of hole acceleration after $\omega_{p_e} t = 280$ (see Fig. 9) can be traced to the plateauing of the electron distribution function as in Fig. 1. Similar to Fig. 5, Fig. 8 shows the wake of phase space density disrupted from the accelerating hole. The initial portion of this disrupted hole mass gets mixed into the background phase space density and disappears by $\omega_{p_e} t = 210$. Similar

to the random start run depicted in Fig. 2, new ion holes emerge out of the background turbulence. One such hole is evident at $(13\lambda_D, 1.25v_{th,i})$ in Fig. 8F, while two others are observed at $(2\lambda_D, 1.25v_{th,i})$ and $(15\lambda_D, 1.5v_{th,i})$ in Fig. 8H. These latter holes tend to collide and coalesce into longer holes (see Figs. 8H - 8L). Despite the absence of any initially prepared electron holes, large amplitude electron holes also develop (see Fig. 11).

Figure 12 shows the deceleration of the initially prepared ion hole for a drift of $v_D = 1.25v_{th,i}$. Note that this drift is *below* the drift for marginal stability observed in Ref. 3 ($v_D = 1.5v_{th,i}$). The loss of hole marker particles evident in Fig. 12B is due to hole decay caused by discrete particle collisions. Figure 13 shows the center marker velocity in time. The initial rise in marker velocity is due to hole ion Landau damping (see Sec. Va) while the subsequent oscillation is due to trapped particle oscillations in the hole potential (see Sec. Va). The steady average deceleration of the center marker as the hole moves to regions of higher ion phase space density is evident.

A plot of the measured isolated hole growth rate γ_H against v_D is shown in Fig. 14. Discrete particle collisions and clump fluctuations were thought to be negligible early in the run when the measurements were made. Moreover, since the growth rate depends on the hole depth, we made the measurements on holes of the same depth. The solid curve in Fig. 14 is a theoretical hole growth rate γ_h discussed in Sec. Va. Note that Fig. 14 implies that an isolated hole grows for *any* finite drift velocity. However, for the clump instability of Fig. 4 in Ref. 3(see also Fig. 19), a marginal point at finite drift is evident. We argue in Sec. Vb that this difference is due to collisions between holes, *i.e.*, the clump instability can only occur if the decay rate resulting from hole-hole collisions can be overcome.

We also made a run with an initial isolated hole where $v_D = 4.2v_{th,i}$, *i.e.*, above the linear stability boundary. As in the linearly stable cases, the isolated ion hole decelerated and grew in amplitude. However, this linearly unstable case is more complicated since linearly unstable waves evolve which interact with the hole. We are studying the hole-wave interaction further and will present the results elsewhere.

c. Effect of Discrete Particle Collisions

Electric fields due to particle discreteness can disrupt hole structure and cause hole decay. We have made a series of runs to asses the effect of discrete particle collisions in the simulations described here and in Ref. 3. We made runs with different particle number N_p, and therefore, different particle collisionality. In each case, an isolated ion hole of size $\tilde{f}/f_0 = -0.6$, $\Delta x = 5\lambda_D$, and $\Delta v = .25v_{th,i}$ was introduced at $v = 0.75v_{th,i}$ into what were otherwise quiet start initial conditions. Ion marker particles were introduced into the hole so that the destruction of the hole by discrete particle collisions could be observed. Comparisons between the various runs were then made after hole equilibration had occurred and the background electrostatic energy had risen to the thermal level. In each of the runs, the electron drift was $v_D = 1.25v_{th,i}$, *i.e.*, v_D was below the point of marginal stability for the clump instability observed in Ref. 3. Therefore, throughout each run, the only fluctuations present were the initially present ion hole and the discrete particle fluctuation level.

Under these conditions, we model the *net* ion hole growth rate as

$$\gamma = \gamma_H + \gamma_d \tag{5}$$

where γ_d is the hole decay rate due to discrete particle collisions. We write γ_d as[4]

$$\gamma_d(n_0\lambda_D) = -\frac{D_i}{\Delta v^2} = -\beta\frac{\omega_{p_i}v_{th,i}^2}{n_0\lambda_D\Delta v^2} \tag{6}$$

where Δv is the hole velocity width and D_i is the ion velocity space diffusion coefficient (the numerical factor β is determined below). Equations (5) and (6) are highly idealized and are used here only for the purpose of *estimating* the magnitude of hole decay by particle collisions. This idealized model assumes that the result of particle collisions is to reduce the hole amplitude by a simple velocity diffusion process. Though the collision process is more complicated than this, we believe that the simplified model embodied in Eqs. (5) and (6) is a meaningful representation of the collisional decay. The simplicity of the model is

useful since γ_H will be the same for each run (we keep the drift, ion hole size, and initial phase space location of the hole fixed). We need only measure γ_H for the different $n_0\lambda_D$ values to obtain γ_d.

Figures 15A - 15C show the final ($\omega_{p_e}t = 560$) ion phase space density for the cases $n_0\lambda_D \approx 407$ (A), 815 (B), 1630 (C), while Fig 12B shows the case $n_0\lambda_D = 3260$. The boundary between hole growth or persistence and hole decay by discrete particle collisions occurs approximately for $n_0\lambda_D \approx 1000$ (between cases described in Figs. 15B and 15C). Using the hole growth rate from Fig. 14 for $v_D = 1.25v_{th,i}$, we have

$$\gamma_H + \gamma_d(3260) \approx 1.0 \times 10^{-3}\omega_{p_e} \tag{7}$$

and

$$\gamma_H + \gamma_d(1000) \approx 0. \tag{8}$$

But Eq. (6) implies that $\gamma_d(1000) = 3\gamma_d(3000)$ so that

$$\gamma_d \approx -5.0 \times 10^{-4}\omega_{p_e} \tag{9}$$

for $n_0\lambda_D \approx 3260$ with fluctuations of size $\Delta v \approx 0.5v_{th,i}$.

Two other methods yield alternate determinations for γ_d. First, we can measure D_i directly by measuring the mean square velocity scatter $\langle \delta v^2 \rangle$ of the hole marker particles in time. As is clear from Fig. 16, the scatter is considerable for the smaller $n_0\lambda_D$. The spread δv satisfies $\langle \delta v^2 \rangle = 2D_i t$ asymptotically, while Eq. (6) implies that D_i decreases with increasing $n_0\lambda_D$. Figure 17 shows the measured values of $\langle \delta v^2 \rangle$ in time for $n_0\lambda_D = 3260$. The slope gives $D_i = 4.9 \times 10^{-4}\omega_{p_e}v_{th,i}^2$ so that, with $\Delta v = 0.5v_{th,i}$, we can use Eq. (6) to obtain

$$\gamma_d \approx -1.97 \times 10^{-4}\omega_{p_e}. \tag{10}$$

In addition, we can evaluate the ion discrete particle diffusion coefficient theoretically by the standard shielded test particle model and obtain

$$D_i = \frac{v_{th,i}^2\omega_{p_i}}{n_0\lambda_D C_2}\left(\frac{\pi}{2} - \tan^{-1}\frac{C_1}{C_2}\right)\left[\frac{v_{th,i}}{(2\pi v_{th,i}^2)^{1/2}}\exp\left(\frac{-v^2}{2v_{th,i}^2}\right) + \frac{v_{th,i}}{(2\pi v_{th,e}^2)^{1/2}}\exp\left(\frac{-(v-v_D)^2}{2v_{th,i}^2}\right)\right]. \tag{11}$$

The parameters C_1 and C_2 are derived from integrals of the dielectric function $\epsilon(k, kv)$ and can be written as

$$C_1 = 2 + \frac{v}{(2v_{th,i}^2)^{1/2}} \mathrm{Re}\, Z(\frac{v}{\sqrt{2}v_{th,i}}) + \frac{v_D - v}{2\sqrt{2}v_{th,i}} \mathrm{Re}\, Z(\frac{v_D - v}{2\sqrt{2}v_{th,i}}) \tag{12}$$

and

$$C_2 = \frac{v}{(2v_{th,i}^2)^{1/2}} \mathrm{Im}\, Z(\frac{v}{\sqrt{2}v_{th,i}}) - \frac{v_D - v}{2\sqrt{2}v_{th,i}} \mathrm{Im}\, Z(\frac{v_D - v}{2\sqrt{2}v_{th,i}}) \tag{13}$$

where $v = 0.625 v_{th,i}$ is the hole velocity and Z is the plasma dispersion function. Evaluating D_i for our case, we find

$$D_i = 0.33 \frac{v_{th,i}^2 \omega_{p_i}}{n_0 \lambda_D} \tag{14}$$

so that $\beta = 0.33$ in Eq. (6). Therefore, for $n_0 \lambda_D = 3260$, we obtain $D_i = 5.28 \times 10^{-4} \omega_{p_e} v_{th,i}^2$ and find a result in approximate agreement with Eq. (10):

$$\gamma_d \approx -2.12 \times 10^{-4} \omega_{p_e}. \tag{15}$$

Since clump-hole fluctuations of size $\Delta v \approx 0.2 v_{th,i}$ were observed in Ref. 3 where $N_p = 102400$ particles per species, we can use Eqs. (6) and (14) to estimate γ_d in Ref. 3 as

$$\gamma_d \approx -1.23 \times 10^{-3} \omega_{p_e} \tag{16}$$

In Sec. Vb, we will use this estimate for γ_d to asses the role of discrete particle fluctuations on the point of marginal stability observed in Ref. 3.

V. Discussion

a. Hole Model

The observations discussed in Sec. IVb and in Ref. 2, provide compelling evidence that a turbulent plasma tends, under a variety of initial conditions, to develop into a collection

of phase space density holes in a background of enhanced phase space density fluid. This occurs because turbulent electric fields will mix the phase space fluid and necessarily produce local depressions (holes; $\delta f \leq 0$) and enhancements ($\delta f \geq 0$) in the phase space density. When the shielding distance λ, given by Eq. (18) is real, a hole tends to self-bind and, when in isolation, forms a trapped particle phase space eddy in BGK equilibrium. The enhanced phase space fluid self-repels and fills the interstitial regions between the holes. The tendency of plasma to form holes can be understood from the fact that a BGK hole is a state of maximum entropy, subject to constraints of constant mass, energy, and momentum[10]. Therefore, a BGK hole equilibrium is a most probable state for the (self-)organization of plasma fluctuation energy, momentum, and mass. Apparently, even in a turbulent plasma, where collisions between holes hinder the development of isolated hole equilibria, BGK holes still tend to form. This is clear from the emergence of isolated holes during the nonlinear instability-driven turbulence described in Sec. IV and the decay turbulence observed in Ref. 2.

Roughly speaking, a hole can be characterized by its depth $\tilde{f}$, its spatial width Δx and its velocity trapping width $2\Delta v_t$. A single hole in isolation can be in equilibrium if its depth and therefore, its potential are sufficient to bind it. For an ion hole, this equilibrium condition is

$$\tfrac{1}{2} m_i \Delta v_{t,i}^2 = e\phi_0 \tag{17}$$

where ϕ_0 is the minimum of the hole potential. We can estimate $\tilde{f}$ by using Eq. (17) and Poisson's equation. The shielding length λ is given by

$$\lambda^{-2} = -\sum_{\text{all species}} \omega_p^2 \mathrm{PV} \int du \, \frac{f_0'(v)}{v-u} \tag{18}$$

(PV means principal value). When $\Delta x \gg \lambda$, Poisson's equation is

$$\lambda^{-2}\phi_0 \approx 4\pi n_i m_i e \tilde{f}_i 2\Delta v_{t,i} \tag{19}$$

Combining Eqs. (19) and (17), we find that

$$\tilde{f}_i \approx -\frac{\Delta v_{t,i}}{4\lambda^2 \omega_{p_i}^2} \tag{20}$$

A more detailed calculation[10] gives a similar value for holes with $\Delta x/\lambda \gg 1$. In particular, for arbitrary $\Delta x/\lambda$, we find that[10]

$$\tilde{f}_i = \frac{\Delta v}{6\omega_{p_e}^2 \lambda^2} g^{-1}\left(\frac{\Delta x}{\lambda}\right) \tag{21}$$

where

$$g(z) = (1 + 2/z)[1 - \exp(-z)] - 2. \tag{22}$$

Once produced, a BGK-like hole can become unstable[10,4], *i.e.*, get deeper, not fall apart. (This instability is not to be confused with the case where a Bernstein-Greene-Kruskal mode can decay by coupling to waves as in, for example, Ref. 12). Consider an ion hole located at velocity u. Since the hole appears to be negatively charged, *i.e.*, it is a region of plasma with a depletion of ions, electrons will be reflected by the ion hole's electric field. If there are more electrons moving faster than the hole than slower, *i.e.*, $f'_{0e}(u) \geq 0$, then reflecting resonant electrons will impart momentum to the hole. Consequently, the ion hole moves (decelerates) to a region of velocity space with larger $f_{0i}(u)$, and therefore, the hole gets deeper, *i.e.*, $f_0 - f = -\tilde{f}$ gets larger since f must remain constant. This situation is represented in Fig. 17.

One can compute the acceleration $\dot{u}$ of the ion hole from momentum conservation. The rate of change of the momentum of the ion hole is

$$M\dot{u} \tag{23}$$

where

$$M \approx 2n_i m_i \tilde{f}_i \Delta x \Delta v_{t,i} \tag{24}$$

is the ion hole mass. As the hole grows, passing ions in a velocity layer $|v - u| \leq \Delta v$ gain momentum at the (approximate) rate

$$\gamma n_i m_i f'_{0i}(u) \Delta v_{t,i}^3 \Delta x. \tag{25}$$

A linear theory calculation would show that the resonant ions gain momentum at the rate (25) with γ replaced by $\Delta v_{t,i}/\Delta x$. For example, equating this result to the rate of change

of wave momentum would give the ion Landau damping rate. However, this linear result is only valid for times t such that $(\Delta v_{t,i}/\Delta x)t < 1$, so we may regard Eq. (25) as the extension of the linear calculation into the nonlinear regime for times longer than a trapping time.

The reflected electrons lose momentum at the rate

$$\pi^{-1}\omega_{p_e}^2\phi_0^2 f'_{0e} \tag{26}$$

which, except for a numerical factor of order unity, is the standard linear theory value of the Fokker-Planck drag. The ion hole acceleration $\dot{u}$ can be obtained if we equate Eq. (23) to the sum of Eqs. (25) and (26). Substituting this value of $\dot{u}$ into

$$\frac{\partial \tilde{f}_i}{\partial t} = \gamma_h^i \tilde{f}_i = -\dot{u} f'_0 \tag{27}$$

and using Eqs. (20) and (24), we can calculate the theoretical hole growth rate γ_h^i. Using $v_{th} = \lambda_D \omega_p$, we obtain

$$\gamma_h^i = -2\frac{\Delta v_{t,i}}{\Delta x}\frac{v_{th,e}^2 f'_{0e}(u) v_{th,i}^2 f'_{0i}(u)}{(\lambda_D/\lambda)^2 + 4[v_{th,i}^2 f'_{0i}(u)]^2}. \tag{28}$$

A more rigorous calculation for equal electron and ion temperatures $T_e = T_i$ gives the growth rate

$$\gamma_h^i = -0.194\frac{\Delta v_{t,i}}{\lambda}\frac{v_{th,e}^2 f'_{0e}(u) v_{th,i}^2 f'_{0i}(u)}{(\lambda_D/\lambda)^2 + 2.24[v_{th,i}^2 f'_{0i}(u)]^2} \tag{29}$$

The detailed calculation also predicts that the growing hole has a length $\Delta x \approx 7\lambda$. When this value of Δx is used in Eq. (28), the approximate γ_h agrees reasonably well with Eq. (29).

A steady sate equilibrium hole (BGK mode) has in addition to the trapped particle momentum $M\dot{u}$, a momentum due to a resonant layer ($|v| \approx \Delta v$) equal to $\frac{1}{3}n_i m_i f'_{0i}(u)\Delta v_{t,i}^3 \Delta x$. This result can be readily obtained by integrating Eq. (25) over time. This effect is apparent in the simulation during the formation of the BGK equilibria from the initial rectangular hole which is imposed at $\omega_{p_e} t = 0$ (see Fig. 7 and the initial rise in hole velocity in Fig. 13). This initial hole is created without the resonant layer required for the BGK equilibria. The subsequent formation of this layer requires a momentum input, which can come only

from changing the hole velocity by an amount Δu. Equating $-M\Delta u$ to the resonant layer momentum and using Eqs. (20) and (24) gives the change Δu in u during the equilibration process

$$\frac{\Delta u}{\Delta v_{t,i}} = -\frac{\pi}{3}\left(\frac{\lambda}{\lambda_D}\right)^2 v_{th,i}^2 f_{0i}' \tag{30}$$

Using this result in $\delta\tilde{f} = -\Delta u f_{0i}'$ gives the relative reduction in hole depth during equilibration

$$\frac{\delta\tilde{f}}{\tilde{f}} = -\frac{8}{3}\left(\frac{\lambda}{\lambda_D}\right)^4 (v_{th,i}^2 f_{0i}')^2 \tag{31}$$

This decay is similar to Landau damping. We observed initial hole decay consistent with Eq. (31) in the simulations. In fact, the decay causes somewhat of a numerical problem since the hole instability growth really begins from an initial state which is the "final" state of the equilibration process. This "final" state can be of very small amplitude because of the decay (31) and consequently can be more affected by discrete particle damping and other noise in the simulations.

If $f_0'(u) \neq 0$ for the non-hole species, *e.g.*, electrons for an ion hole, then an electric field and a potential drop will occur across the hole. It is this field which accelerates the hole and leads to its growth. This potential structure is sometimes referred to as a double layer. The potential and electric field structure assoicated with an unstable ion hole are depicted in Fig. 18. We can calculate the magnitude of the potential drop $\delta\phi = \phi(x = +\infty) - \phi(x = -\infty)$ as follows. At $|x| = \infty$, $\partial^2\phi/\partial x^2 = 0$, so Poisson's equation may be written as

$$\lambda^{-2}\phi(x) = 4\pi ne \int dv\, \delta f \tag{32}$$

where δf is the perturbation in the distribution function due to reflected particles. Consider an ion hole. Electrons in a stream of velocity width $\Delta v_{t,i}$ are reflected from the hole. As a consequence, at $x = -\infty$,

$$\delta f(v) = \begin{cases} -2v f_{0e}'(u) & \text{for} \quad -\Delta v_{t,i} \leq v - u \leq 0, \\ 0 & \text{otherwise,} \end{cases} \tag{33}$$

and at $x = +\infty$

$$\delta f(v) = \begin{cases} -2v f'_{0e}(u) & \text{for} \quad \Delta v_{t,i} \geq v - u \geq 0, \\ 0 & \text{otherwise.} \end{cases} \tag{34}$$

Using these expressions for $\delta f(v)$ in Eq. (32), along with (17), we find

$$\frac{\delta\phi}{\phi_0} = -\left(\frac{\lambda}{\lambda_D}\right)^2 v_{th,e}^2 f'_{0e}(u) \tag{35}$$

We have measured the potential drop across the hole in the simulations and found it to be generally consistent with Eq. (35).

b. Clump Model

The clump model is concerned with the opposite extreme to that of isolated holes in the hole model, *i.e.*, it is concerned with the case where a large fraction of the available phase space is occupied by holes. In this case, the hole packing fraction p is near $\frac{1}{2}$ and collisions between holes become prevalent. The hole-hole collisions mix the phase space density and thereby produce new holes (clumps) throughout the phase space. In this way, a fully developed turbulent state emerges. Such a system is amenable to a statistical description (Ref. 7). However, rather than reviewing the statistical theory of clump turbulence, we find it enlightening here to consider clump turbulence in terms of the hole model. As we shall see, the hole model forms the essential physical building blocks of the clump model. We will view clump turbulence as a random collection of interacting BGK-like holes. In this way, the clump instability can be seen to be the many fluctuations analog of the isolated hole instability.

We can model the effect of hole-hole collisions on the growth rate of an isolated ion hole by

$$\gamma = \gamma_h^i + \gamma_{hh} \tag{36}$$

where $\gamma_{hh} = -2pr(\Delta v/\Delta x)_i$ is the net hole-hole collision rate. Equation (36) is analogous to Eq. (5) which describes the effect of hole decay by discrete particle collisions. The factor

$r \leq 1$ models the tendency of holes to attract each other and recombine. The appearance of the packing fraction p in Eq. (36) takes into account the fact that the collision rate between holes is proportionally reduced as the hole packing fraction is reduced. In the case of the clump model, $p = \frac{1}{2}$ and, as a consequence, holes resulting from the mixing of the phase space density have velocity widths Δv and spatial scales $\Delta x = k^{-1}$ related to the ion diffusion coeficient D_i by the mixing length, *i.e.*, $\Delta v = (D_i/3k)^{(1/3)} = k^{-1}/\tau_i$. For $p = \frac{1}{2}$, Eq. (36) corresponds to the following equation for the two-point fluctuation correlation function evaluated at ($x_- = 0$, $v_- = 0$)

$$\left(\frac{\partial}{\partial t} + \frac{r}{\tau_i}\right)\langle \delta f_i^2 \rangle = -2\gamma_h^i \langle \delta f_i^2 \rangle. \tag{37}$$

The right-hand side of Eq. (37) describes ion hole growth while the r/τ_i term models the decay of the self-binding holes by hole-hole collisions. Using Eq. (28), we can write the right hand side of Eq. (37) as $-2\langle \dot{u}\delta f_i \rangle f_{0i}'$ where $\dot{u}$ is the ion hole acceleration due to the reflection of resonant electrons. In a turbulent plasma, $\dot{u}$ is a fluctuating quantity and $\langle \dot{u}\delta f_i \rangle f_{0i}^{-1}$ is the ion Fokker-Planck drag F^{ie} due to the electrons. Equation (37) can be written as

$$\left(\frac{\partial}{\partial t} + \frac{r}{\tau_i}\right)\langle \delta f_i^2 \rangle = -2F^{ie} f_{0i} \frac{\partial f_{0i}}{\partial v}. \tag{38}$$

Equation (38) is incomplete in its description of clump dynamics, since it does not take into account the source of new clumps (holes) that result from the random mixing of the average phase space density. In order to obtain this effect, we note that since the phase space density is conserved,

$$\frac{\partial}{\partial t}\int dv\,(\langle \delta f^2 \rangle + f_0^2) = 0. \tag{39}$$

If we now assume that the average density $f_0(v)$ satisfies a Fokker-Planck equation

$$\frac{\partial f_0}{\partial t} = \frac{\partial}{\partial v} D \frac{\partial}{\partial v} f_0 - \frac{\partial}{\partial v} F f_0, \tag{40}$$

then Eq. (39) becomes

$$\frac{\partial}{\partial t}\int dv\,\langle \delta f^2 \rangle = \int dv \left[2D\left(\frac{\partial f_0}{\partial v}\right)^2 - 2F f_0 \frac{\partial f_0}{\partial v}\right] \tag{41}$$

The second term on the right hand side of Eq. (41) corresponds to the coherent acceleration term on the right hand side of Eq. (38). The D-term in Eq. (41) describes the production of clumps by the random mixing of the average phase space density. This mixing process requires an additional term to be added to Eq. (38), *i.e.*, Eq. (38) becomes

$$\left(\frac{\partial}{\partial t}+\frac{r}{\tau_i}\right)\langle\delta f_i^2\rangle = 2D^{ie}\left(\frac{\partial f_{0i}}{\partial v}\right)^2 - 2F^{ie}f_{0i}\frac{\partial f_{0i}}{\partial v} \tag{42}$$

where D^{ie} is the ion diffusion coefficient due to the electric fields of the electrons. The dynamical equation for electron clumps follows by exchanging labels e and i in Eq. (42).

The statistical theory of clump fluctuations derives a renormalized equation for the two-point fluctuation correlation function $G^\alpha(x_-, v_-) = \langle\delta f^\alpha(1)\delta f^\alpha(2)\rangle$ for species α. Neglecting self-binding effects, G^α satisfies[7]

$$\left(\frac{\partial}{\partial t}+v_-\frac{\partial}{\partial x_-}-\frac{\partial}{\partial v_-}D_-\frac{\partial}{\partial v_-}\right)G^\alpha = S^\alpha \tag{43}$$

where the source term is

$$S^\alpha = 2D_{12}^{\alpha\beta}(f'_{0\alpha})^2 - 2F_{12}^{\alpha\beta}f_{0\alpha}f'_{0\alpha}. \tag{44}$$

These two equations (43) and (44) are the clump theory equations corresponding to the qualitative result (42). The diffusion coefficient $D_-(x_-)$ in Eq. (43) describes the relative diffusion between two phase space points and therefore, vanishes as $x_- \to 0$. In the clump theory, the D_- term in Eq. (43) is the analog of the hole-hole collision rate γ_{hh}.

Together, the free streaming and velocity diffusion operators on the left hand side of Eq. (43) lead to stochastic instability of neighboring particle orbits. This destruction of fluctuations (correlations) is modeled approximately in Eq. (42) by the $r\tau_i^{-1}$ term. In order to see this in detail, we take moments of the left hand side of Eq. (43) and find that

$$\frac{\partial^3}{\partial t^3}\langle x_-^2\rangle = 2\langle D_-(x_-)\rangle = 2k_0^2D\langle x_-^2\rangle \tag{45}$$

where

$$k_0^2 = \frac{1}{2D}\left(\frac{\partial^2}{\partial x_-^2}D_-\right)_{x_-=0} \tag{46}$$

determines the mean square spatial scale of the turbulence. The solution of Eq. (45) for initial values $x_-(0) = x_-$, $v_-(0) = v_-$ gives an exponential separation for neighboring particle orbits, *i.e.*,

$$\langle x^2{}_-(t)\rangle = \tfrac{1}{3}(x_-^2 - 2x_-v_-\tau_0 + 2v_-^2\tau_0^2)e^{t/\tau_0} \tag{47}$$

where $\tau_0 = (4k^2D)^{-1/3} = (12)^{-1/3}\tau$ is a characteristic time sometimes referred to as the Liapanov time. The clump lifetime $\tau_{cl}(x_-, v_-)$ is defined as the time for two orbits, initially separated by (x_-, v_-) to separate spatially by the typical clump size k_0^{-1}:

$$\tau_{cl}(x_-, v_-) = \tau_0 \ln\left[\frac{3}{k_0^2(x_-^2 - 2x_-v_-\tau_0 + 2v_-^2\tau_0^2)}\right]. \tag{48}$$

As we have noted, although an individual fluctuation is destroyed (by orbit stochastic instability) at a rate $\tau_{cl}(x_-, v_-)^{-1} \approx \tau^{-1}$, the recombination feature of the holes leads to a net fluctuation decay rate that is *less* than τ_{cl}^{-1} (*c.f.* Ref. 2). At present, the clump theory has no analytical derivation for this effect. The use of the τ factor to model hole recombination in Eq. (42) is phenomenological, but appears to be supported by the simulations of Ref. 2 where it was found for decay turbulence that $\tau \approx 0.3$.

The clump growth rate can be calculated from the model equations (43) and (46). A detailed calculation is carried out in Ref. 5. It is found that the instability grows on the τ_0 time scale and has a finite drift velocity threshold. The finite marginal point is due to the competition between collisions among self-binding holes (τ/τ_0) and the clump source term (S_{12}) due to phase space mixing and hole acceleration.

c. Comparision Between Simulation and Theory

The hole model compares favorably with the simulation results. For example, we note that the phase space structure of the holes observed in Sec. IV is consistent with the hole model. We consider the ion hole at $v = 0$ in Fig. 8F. It has a scale length $\Delta x \approx 2.6\lambda_D$ and $\Delta v \approx 0.75 v_{th,i}$ whereas its depth (see Fig. 10 at $\omega_{p_e}t = 180$) is $\tilde{f}/f_{0i}(0) \approx -0.9$. Using Eqs. (21) and (22), we see that the hole in Fig. 8F is consistent with the hole model. However,

the hole in Fig. 8F has a scale length ($2.6\lambda_D$) that is somewhat smaller than that predicted for the most probable state in the hole model[10] ($7\lambda_D$). This discrepency is most likely due to the decay effects of other fluctuations in the plasma. The hole wake in Fig. 8 is evidence for this decay. In the case of the quiet start runs in Fig. 8, the fluctuations causing the hole decay when $\omega_{p_e}t \leq 200$ are small velocity scale clump fluctuations (see Ref. 3), since shielded discrete particle fluctuations are only fully developed when $\omega_{p_e}t \geq 200$. Note that the holes in the random start run in Fig. 2 are even smaller in Δx than those in Fig. 8. Both hole-hole and discrete particle collisions are hindering hole formation and growth in Fig. 2.

The qualitative features of hole growth observed in Sec. IV are also consistent with the hole model. For example, Eqs. (21) and (29) predict that: (a) hole growth will occur when $f'_{0e}f'_{0i} \leq 0$, while hole decay will occur when $f'_{0e}f'_{0i} \geq 0$ (see Figs. 1 and 8 – 10); (b) the hole growth rate increases with drift v_D (see Fig. 14) and amplitude (see Figs. 2 and 5); (c) the acceleration of an ion hole ceases when $f'_{0e} = 0$ (the electron distribution function plateaus for $\omega_{p_e}t \geq 280$ in Fig. 9); and (d) both Δv and $\tilde{f}_i$ increase (decrease) as the hole grows (decays) (see Figs. 8 and 10). A further confirmation of the model lies in the threshold drift for instability in the random start runs, and the lack of such a threshold in the isolated hole starts. In the latter case, only $f'_{0e}f'_{0i} \leq 0$ is required for instability, whereas in the former case, hole-hole collisions hinder hole growth so that a threshold drift is required for instability. Hole-hole collisions are prevalent in the random start runs since, as discussed in Sec. IVa, $P(\overline{\delta f})$ was Gaussian ($p \approx \frac{1}{2}$) in the early stage of the instability. Of course, discrete particle collisions will lead to a threshold for instability in both the $p \approx \frac{1}{2}$ and $p \ll \frac{1}{2}$ cases (see Sec. IVc).

More detailed comparisions between the simulation results and the model can be made. Using the parameters characteristic of the growing holes observed in Sec. IVb, we can compare γ_h derived from Eq. (29) with the observed growth rates γ_H. This has been done in Fig. 14 where the solid curve is the solution to Eq. (29) with $2\Delta v_{t,i} = \Delta v = 0.75 v_{th,i}$ (the

full velocity width of the ion hole). Except for the larger drifts, the agreement is quite good. For drifts $v_D \geq 3.5 v_{th,i}$ the assumptions underlying Eq. (29) break down. In particular, $\gamma\tau$ and $\omega_{p_e}^2 \lambda^2 f_{0r}'$ are no longer small. The extension of Eq. (29) into this region will be discussed in a future publication.

The decay rate for the clump instability observed in Ref. 3 is due to both discrete particle collisions and hole-hole collisions. From Sec. IVc, we recall that the decay rate due to discrete particle fluctuations is estimated to be on the order of $10^{-3}\omega_{p_e}$ for the simulations in Ref. 3. According to Fig. 4 of Ref. 3, the measured net decay rate for the fluctuations observed in Ref. 3 is on the order of $4.0 \times 10^{-3}\omega_{p_e}$. Therefore, we estimate a decay rate due to hole-hole collisions to be $\gamma_{HH} \approx -3.0 \times 10^{-3}\omega_{p_e}$. This value of γ_{HH} is consistent with the theoretical model since, using Eq. (36) and $\tau_i \approx 80\omega_{p_e}^{-1}$ from Ref. 3, we find that $-\gamma_{HH} \approx \tau_{cl}^{-1} \leq \tau_0^{-1} \approx rD/\Delta v^2 \approx r\tau_i^{-1} \approx \frac{1}{3}(80\omega_{p_e}^{-1})^{-1}$. Therefore, a calculation of the clump growth rate neglecting discrete particle collisions will be in approximate agreement with the measurements of Ref. 3 since $\gamma_{HH} \approx 3\gamma_d$ (see Ref. 5). These approximate calculations imply that the marginal point observed in Ref. 3 and the random start runs of Sec. IVa was due mainly to hole-hole collisions rather than to discrete particle collisions.

As we have already seen in Sec. IVb, the measurements leading to Fig. 14 do not exhibit a similar marginal point at finite drift velocity. This occurs because $\gamma_{HH} = 0$ for an isolated hole and γ_d was negligible during the early stages of the runs ($\omega_{p_e} t \leq 200$). In Fig. 19, we have made a comparison between the isolated hole and clump growth rates. The dots in Fig. 19, are twice the measured growth rates of Fig. 14 for isolated holes. The factor of two was chosen so that the conditions of the isolated hole measurements would correspond to those of the clump measurements of Ref. 3. For example, the results in Ref. 3 were obtained at a time during the runs when $\left\langle \bar{f}^2 \right\rangle^{1/2} / f_0 \approx 10^{-1}$ and $P(\overline{\delta f})$ was Gaussian (*i.e.*, $\left\langle \bar{f}^2 \right\rangle = \bar{f}^2$), whereas for the isolated holes, $\bar{f}/f_0 \approx -0.5$ when the growth rates were measured. Therefore, in order to make comparisons at the *same* constant amplitude, we should multiply the isolated hole data of Fig. 14 by $(0.1/0.5) = 0.2$. Secondly, $\partial\langle \delta N^2 \rangle / \langle N \rangle / \partial t$

is plotted for the instability runs of Ref. 3. Since $\partial\langle\delta N^2\rangle/\partial t \approx \partial\tilde{f}^4/\partial t$, we also need to multiply the growth rates of Fig. 14, by four. Another correction occurs because the clump instability is driven by D and F' terms on the right hand side of Eq. (13), whereas the isolated hole instability is driven by F' only. Since the D and F' terms are comparable at marginal stability, we multiply the isolated hole growth rate by a factor of two. As a final correction, we note that, for a mass ratio of four, the clump instability grows on a time scale somewhat intermediate between τ_e and $\tau_i = 2\tau_e$. These four corrections imply that, in order to compare the isolated hole growth rate measurements of Sec. IVb with the clump growth rate measurements of Ref. 3, we need to multiply the isolated hole growth rates by a factor on the order of two. As is evident from Fig. 19, the two growth rates are consistent with the hole-clump model discussed in this Section and in Sec. Va, *i.e.*, the clump instability is the many interacting hole analog of the isolated hole instability.

VI. Relevance to Laboratory and Space Plasma

Although the nonlinear plasma phenomena reported here is one dimensional and driven by velocity gradients, we believe that similar effects will occur in magnetized plasmas with a spatial density gradient. However, even the one dimensional simulation discussed here has immediate relevance. For example, it is generally believed that current driven electrostatic field fluctuations that propagate parallel to the magnetic field lines are not important for confinement of a current driven plasma. The reason usually given is that ion acoustic waves are linearly stable for present plasma parameters ($T_e \approx T_i$, $v_D \leq 4v_{th,i}$). However, as we have discussed above, hole-clump instability can occur for $T_e \approx T_i$ and for drift velocities significantly below those required for linear instability. Indeed, the simulations with isolated holes discussed in Sec. IVb indicate that, neglecting discrete particle collisions, the isolated hole instability can occur for any finite drift velocity. Therefore, in a plasma with low collisionality – as would be expected of a fusion device – the isolated hole instability is likely

to occur. Its presence would have two notable features. First, since clumps are particle-like fluctuations with phase speeds $\omega/k \leq v_{th}$, we expect a more continuous frequency spectrum with broader phase velocity width than that characteristic of ion acoustic turbulence. This will occur because wave fluctuations, unlike clumps, are plasma normal modes with a definite relation between frequency and wave number, *i.e.*, waves have a discrete frequency spectrum. A second signature of the instability would be the appearance of an anomalous parallel electric resistivity for T_e/T_i parameters and drift velocities in the linearly stable region. Given the complexity of laboratory plasma, it may be difficult to identify and confirm the existence of these features.

The stability of ion acoustic waves when drift velocities are small has also been an issue in the understanding of auroral phenomena[6]. The S3-3 satellite data has shown that double layers exist on auroral magnetic field lines at altitudes of some 7000 km. The double layers are on the order of $32\lambda_D$ long and are separated from each other along the field lines by distances of some $10^3\lambda_D$. An explanation for the existence of these double layers has been of interest. One prominent theory involves the production of double layers from ion holes observed during the simulation of *linear* ion acoustic instability[6]. However, given the experimental error, the measured values of T_e/T_i and v_D in the auroral region may be more consistent with stability than instability of ion acoustic waves. The hole-clump instability appears to be a more likely candidate. For example, the observations are consistent with the evolved state of the clump instability or an emerging state of the isolated hole instability. In the former case, clumps will go unstable for $T_e \approx T_i$ and drift velocities larger than one fifth of that required for linear ion acoustic instability and, as discussed in Sec. IVa, isolated holes will intermittently appear and grow out of the background clump turbulence. In the latter case, isolated holes can appear and grow out of thermal fluctuations for any finite current. In either case, the holes will be intermittent with small packing fractions. (Note that the holes observed from S3-3 have a small packing fraction on the order of $32/1000 \approx 3.2 \times 10^{-2}$). Moreover, as we have discussed in Sec. IVa, unstable ion holes are

double layers - the acceleration of an ion hole is due to the potential drop across the hole which results from the difference in electrons reflected by the hole (see Figs. 17 and 18).

Hole and clump instability may also be relevant to reconnection processes in the earth's magnetotail. In the past, linear ion acoustic turbulence has been one of the mechanisms invoked to explain the anomalously large magnetic reconnection rates believed to be responsible for magnetospheric substorms[13]. While conditions in the plasma current sheet are apparently incomptabable with linear ion acoustic instability, the conditions are consistent with hole or clump instability. Actually, hole or clump instability may be relevant as an anomalous dissipation mechanism in a wide range of magentic field-reversed configurations.

Acknowledgments

It is a pleasure to thank Mr. J. Cook of the Research Laboratory for Electronics photography section at M.I.T. for his expertise in preparing the numerous phase space pictures for this paper. In addition, we would like to thank Drs. T. Chang, G. Crew, M. Hudson, and W. Lotko for discussions on the auroral problem.

This work was supported by the U.S. Department of Energy, the National Science Foundation, and the U.S. Office of Naval Research. Certain calculations were performed with Macsyma at M.I.T.

References

1 T.H. Dupree, *Phys. Fluids*, **15**, 334 (1972).

2 R.H. Berman, D.J. Tetreault, and T.H. Dupree, *Phys. Fluids*, **26**, 2437 (1983).

3 R.H. Berman, D.J. Tetreault, T.H. Dupree, and T. Boutros-Ghali, *Phys. Rev. Let.*, **48**, 1249 (1982).

4 T.H. Dupree, *Phys. Fluids*, **26**, 2460 (1983).

5 D.J. Tetreault, *Phys. Fluids*, **26**, 3247 (1983).

6 M.K. Hudson, W. Lotko, I. Roth and E. Witt, *J. Geophys. Res.*, **88**, 916 (1983).

7 T. Boutros-Ghali and T.H. Dupree, *Phys. Fluids*, **25**, 1839 (1981).

8 T. Boutros-Ghali and T.H. Dupree, *Phys. Fluids*, **25**, 874 (1982).

9 R.W. Hockney and J.W. Eastwood, 1981, *Computer Simulation Using Particles*, (McGraw Hill: New York).

10 T.H. Dupree, *Phys. Fluids*, **25**, 277 (1982).

11 H.L. Berk, C.E. Nielson, and K.V. Roberts, *Phys. Fluids*, **13**, 980 (1970).

12 Kruer, W.L, Dawson, J.M., and Sudan, R.N., *Phys. Rev. Lett.*, **23**, 838 (1969).

13 Papadopulos, K., 1979, in *Dynamics of the Magnetosphere*, ed. S. Akasofu (D. Reidel: New York), 289.

Figures

Fig. 1. The ion and drifting electron spatially averaged distribution functions at times $\omega_{p_e} t = 0$ (dashed line) and 260 (solid line) for the case of a linearly stable random start run with drift $v_D = 3.5 v_{th,i}$.

Fig. 2. A time sequence of the ion phase space for the random start run of Fig. 1. Fig. 2A is the initial state while the sequence starts at $\omega_{p_e} t = 230$ (Fig. 2B) with an interval of $10\omega_{p_e}^{-1}$ between subsequent pictures. In this, and subsequent Figures, the x-axis is the normalized position x/λ_D shown between 0 and 32, while the y-axis is normalized velocity $v/v_{th,i}$. The spontaneous emergence, acceleration (growth), and subsequent decay of isolated (intermittent) phase space holes is apparent.

Fig. 3. The normalized skewness $s(t, v)$ of the probability distribution function of fluctuation ampltiudes $P(\overline{\delta f})$ for the random start run of Figs. 1 and 2. The significant negative skewness is consistent with the hole intermittency in Fig. 2.

Fig. 4. The probability distribution function of fluctuation amplitudes $P(\overline{\delta f})$ at $v = 0$ in the ion distribution function for the random start run of Figs. 1 - 3. $P(\overline{\delta f})$ evolves from a nearly Gaussian distribution at $\omega_{p_e} t = 180$ (a) to one with significant negative skewness at $\omega_{p_e} t = 240$ (b) as an ion hole decelerates through $v = 0$.

Fig. 5. A time sequence of the ion phase space for a linearly unstable, random start run where $v_D = 4.2 v_{th,i}$. The emergence and deceleration of an ion phase space hole is apparent as passive marker particles become trapped in and are carried by the hole.

Fig. 6. The electron phase space for the simulation of Fig. 5. showing a hole coalescing event.

Fig. 7. A time sequence of the ion phase space for a linearly stable run showing the

equilibration of an initially prepared ion hole at $\omega_{p_e}t = 20$ (A), $\omega_{p_e}t = 40$ (B), $\omega_{p_e}t = 60$ (C), $\omega_{p_e}t = 80$ (D), and $\omega_{p_e}t = 100$ (E).

Fig. 8. A time sequence of the ion phase space for a linearly stable case with an initially prepared isolated ion hole (A) and $v_D = 3.0v_{th,i}$. The sequence starts at (B), when $\omega_{p_e}t = 120$, with $10\omega_{p_e}^{-1}$ between figures. (The figure for $\omega_{p_e}t = 150$ is excluded. Thus, 8G shows the ion phase at $\omega_{p_e}t = 180$.) The acceleration and growth of the ion hole is evident.

Fig. 9. The velocity $v(t)$ of a passive marker particle placed at the center of the isolated hole in Fig. 8. The marker particle stays trapped in the hole and can be identified with the hole velocity $u(t)$.

Fig. 10. The normalized ion hole depth $-\tilde{f}(t)/f_0[u(t)]$ for the isolated hole run of Figs. 8 and 9.

Fig. 11. The electron phase space at $\omega_{p_e}t = 240$ for the isolated hole run of Figs. 8 - 10.

Fig. 12. The ion phase space for a linearly stable, isolated hole run with $v_D = 1.25v_{th,i}$ at $\omega_{p_e}t = 40$ (a) and $\omega_{p_e}t = 540$ (b).

Fig. 13. The velocity $v(t)$ of a passive marker particle placed at the center of the initial isolated hole run of Fig. 12.

Fig. 14. The measured isolated hole growth rate γ_H as a function of electron drift v_D. The solid line is the theoretical growth rate γ_h obtained from Eq. (29).

Fig. 15. The breakup of an initially prepared ion hole filled with passive marker particles is shown in the final ion phase space ($\omega_{p_e}t = 540$) for three runs ($v_D = 1.25v_{th,i}$) with different discrete particle collisionality: (A) $n_0\lambda_D = 407$, (B) $n_0\lambda_D = 815$, and (C) $n_0\lambda_D = 1630$. The case for $n_0\lambda_D = 3259$ is shown in Fig. 12B.

Fig. 16. The mean square velocity dispersion $\langle \delta v^2(t) \rangle$ for ion marker particles described in Fig. 15. The slope measures the discrete particle diffusion coeficient that causes the hole decay evident in Fig. 15.

Fig. 17. A schematic picture of the deceleration and growth of an ion hole due to the reflection of electrons by the hole in a region where ion and electron velocity gradients are opposing.

Fig. 18. The potential $\phi(x)$ and electric field $-\partial\phi(x)/\partial x$ shown schematically for an unstable hole.

Fig. 19. The isolated hole data of Fig. 14 (dots) compared with the random start growth rates of Fig. 4 of Ref. 3. The data of Fig. 14 have been corrected in order to correspond to the same fluctuation amplitudes of Ref. 3.

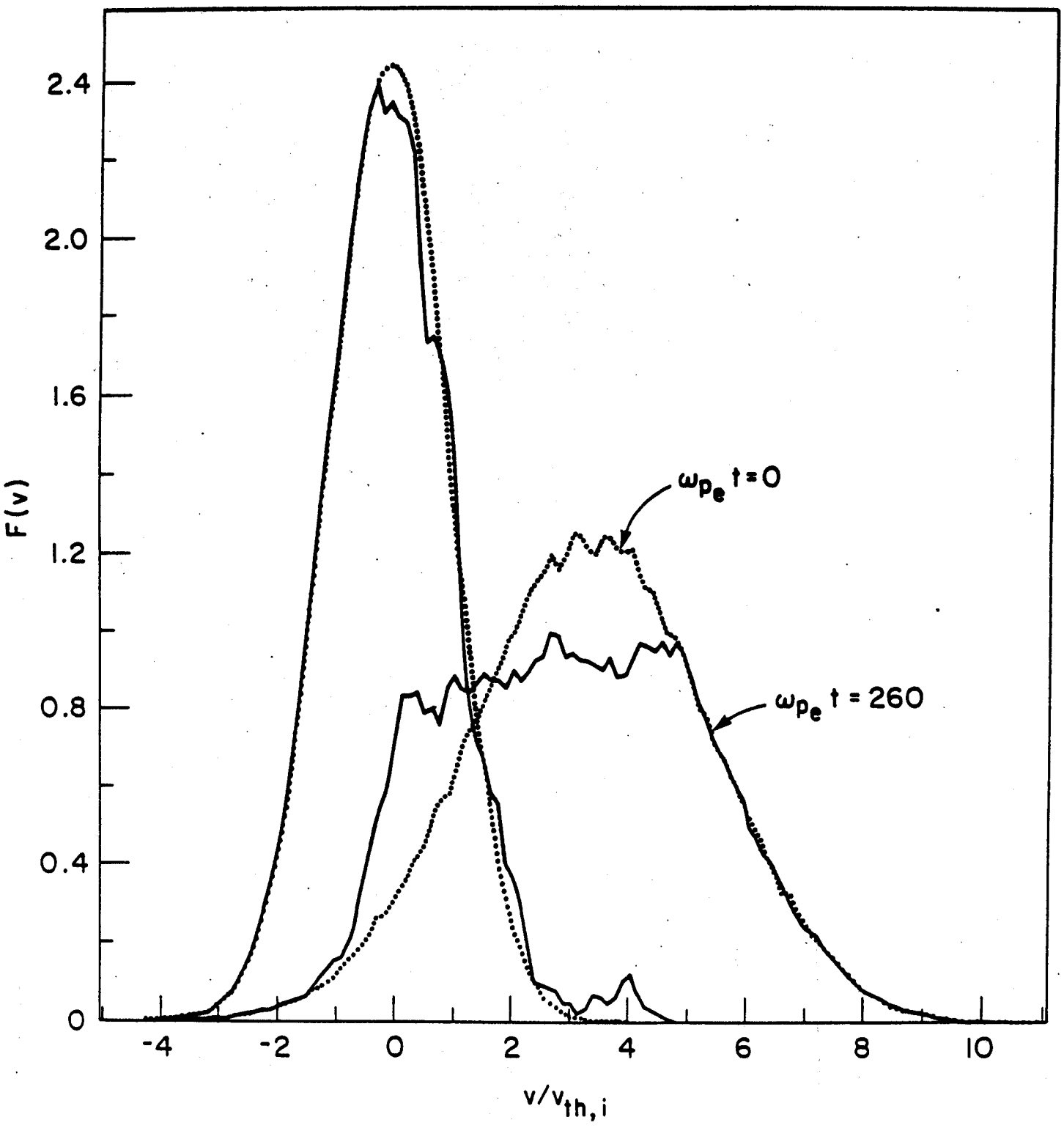

FIGURE 1

A B C

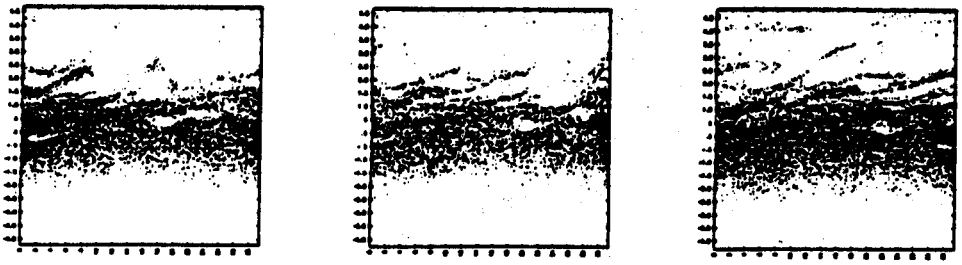

G H I

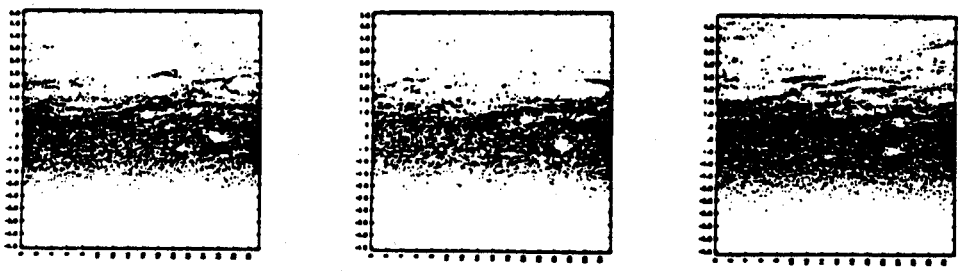

M N O

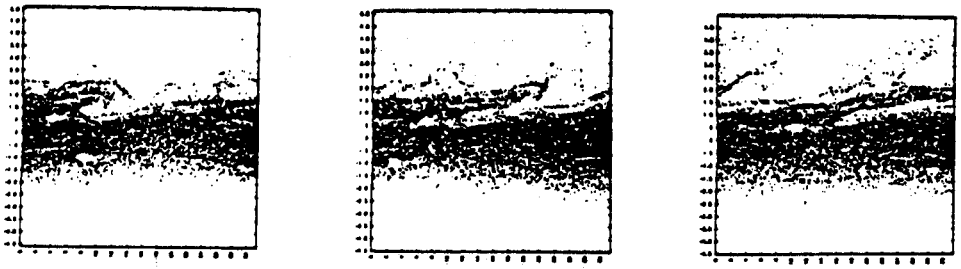

S T U

FIGURE 2

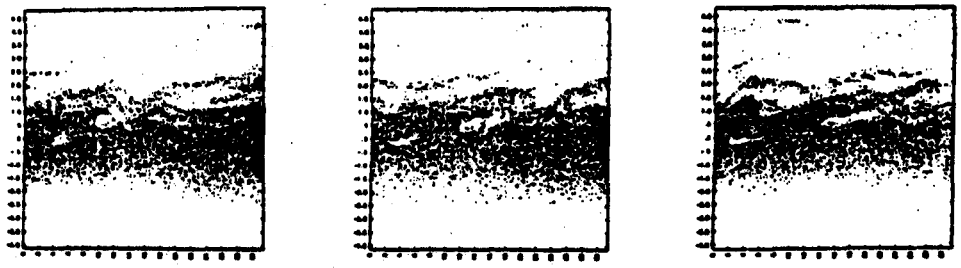

D E F

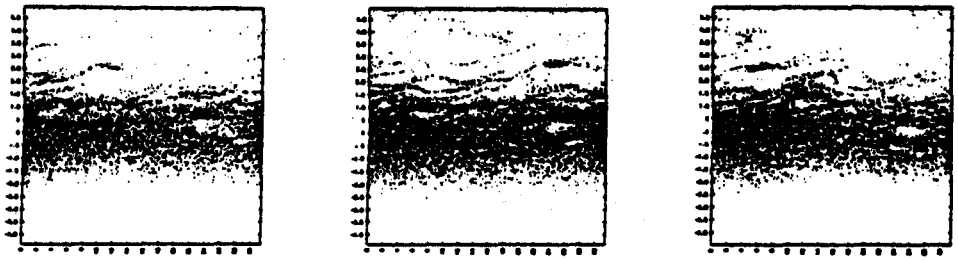

J K L

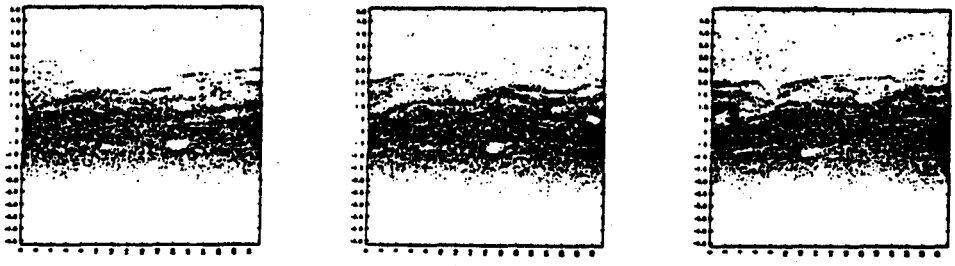

P Q R

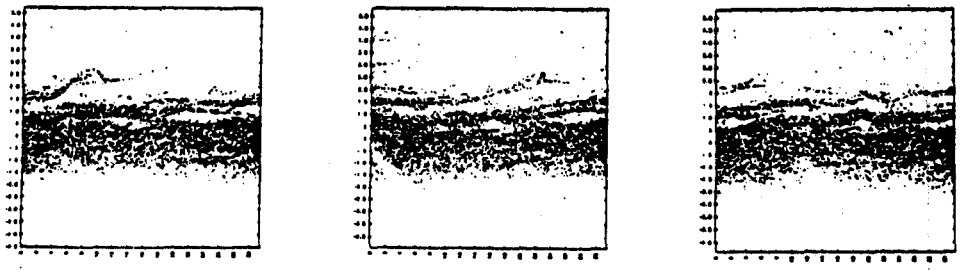

V W X

FIGURE 2 (continued)

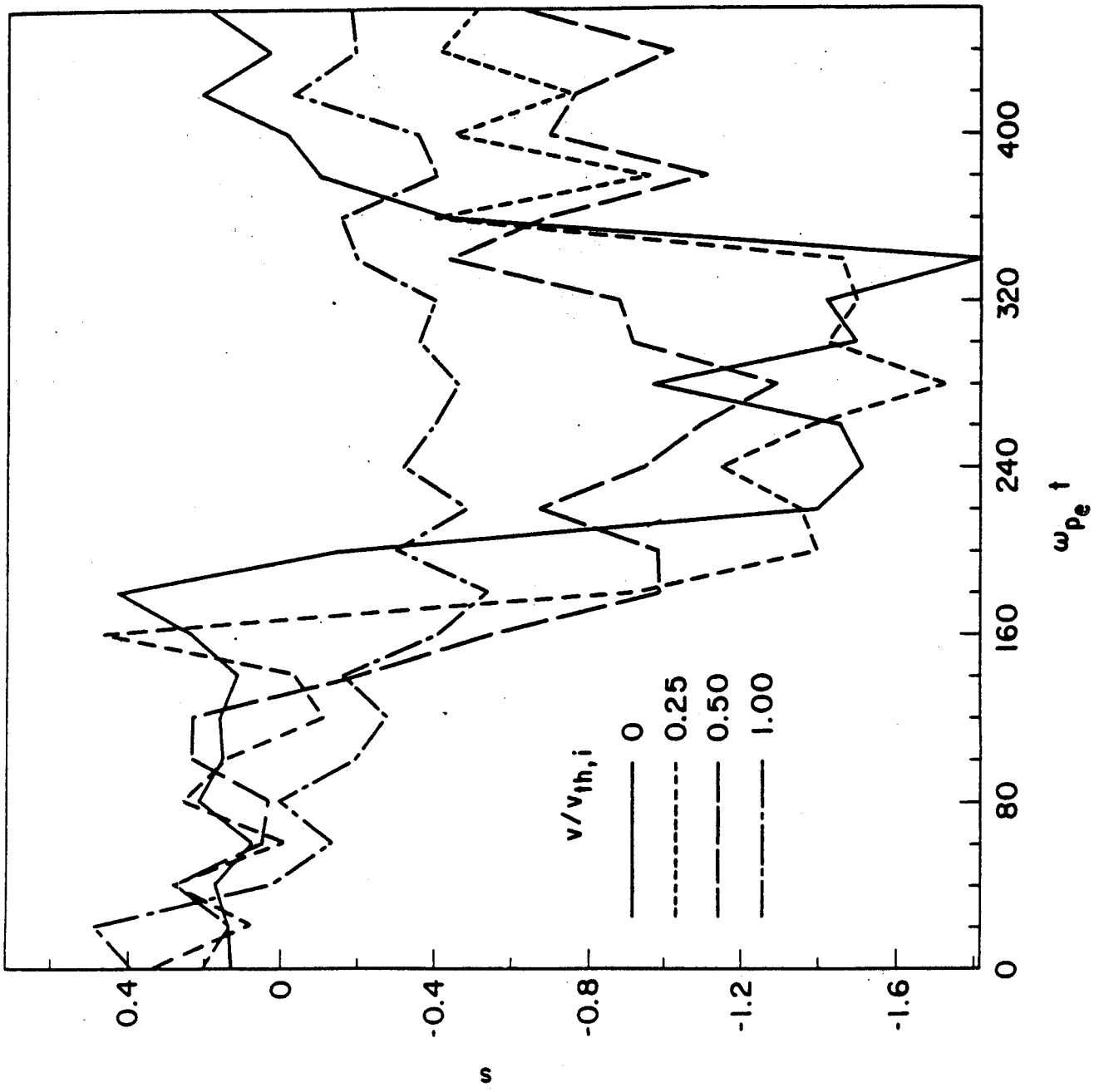
0.4
0
-0.4
-0.8
-1.2
-1.6
s
0
80
160
240
320
400
ω_{pe} t
$v/v_{th,i}$
0
0.25
0.50
1.00

FIGURE 3

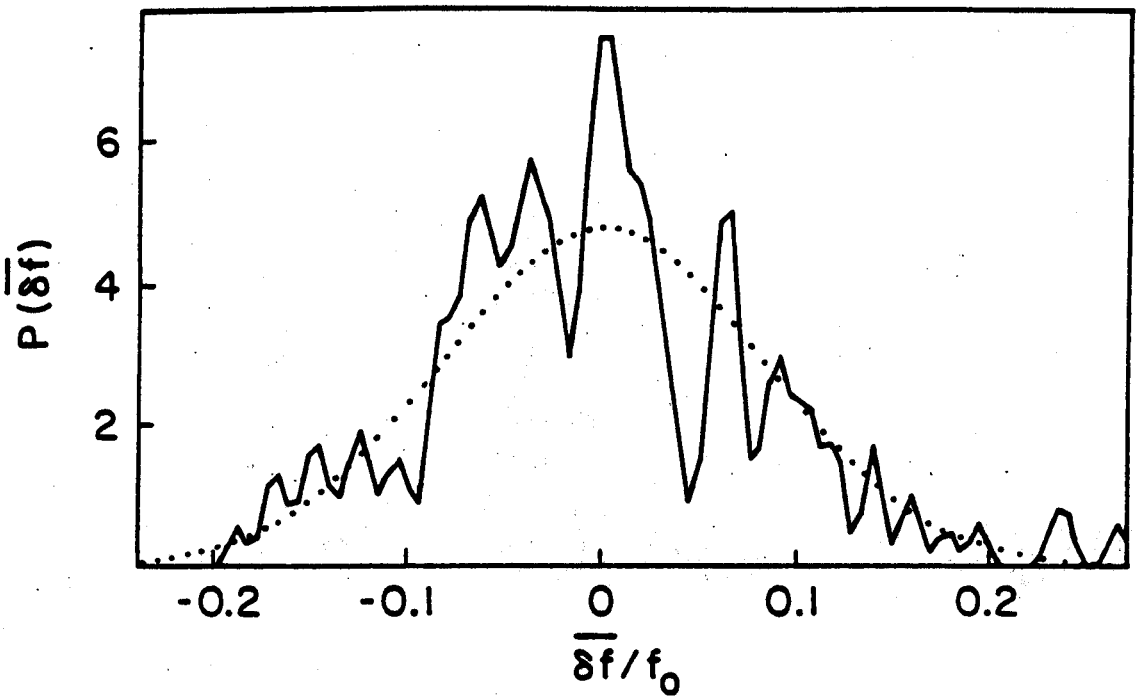

(a)

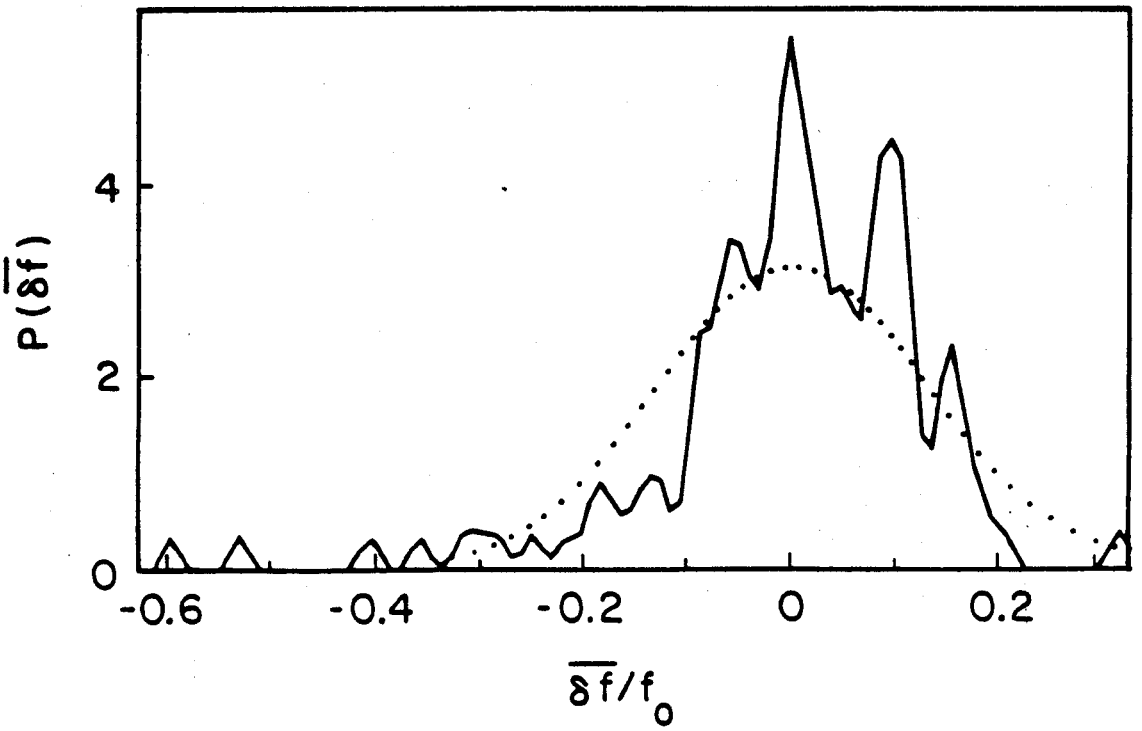

(b)

FIGURE 4

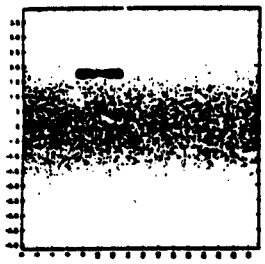

A

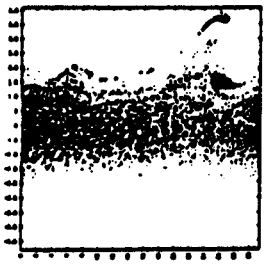

B

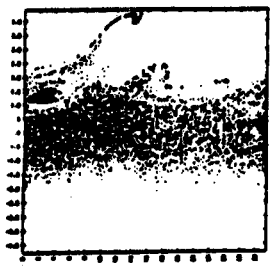

C

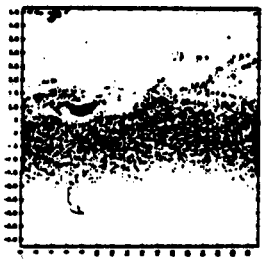

D

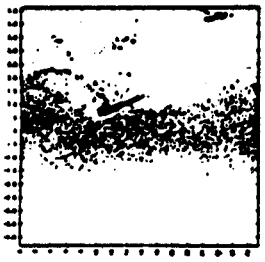

E

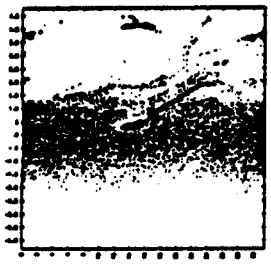

F

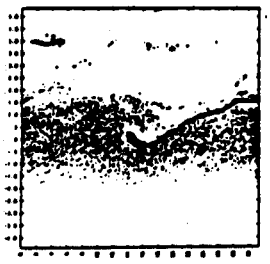

G

H

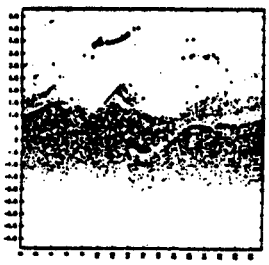

I

J

FIGURE 5

FIGURE 6

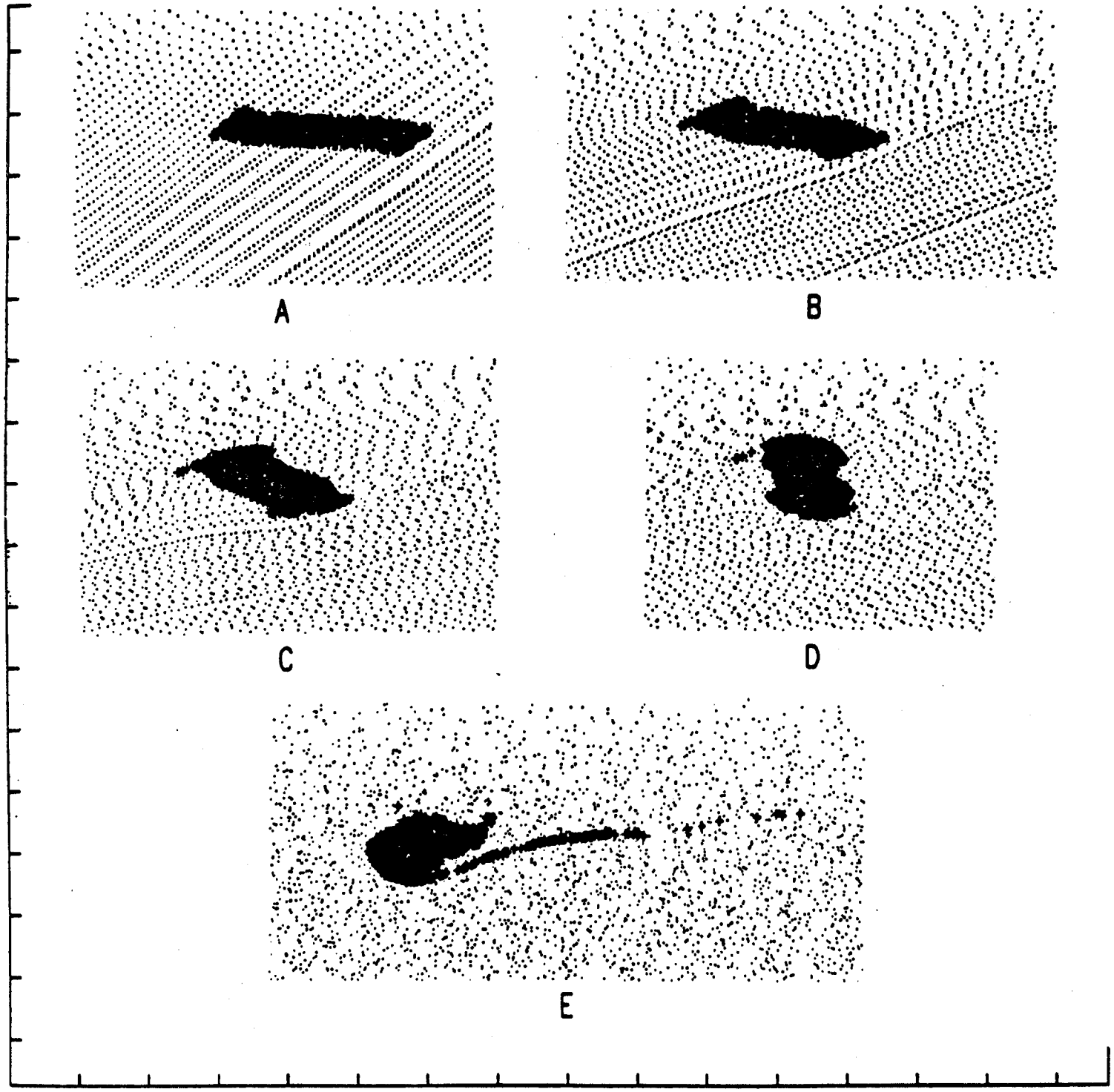

FIGURE 7

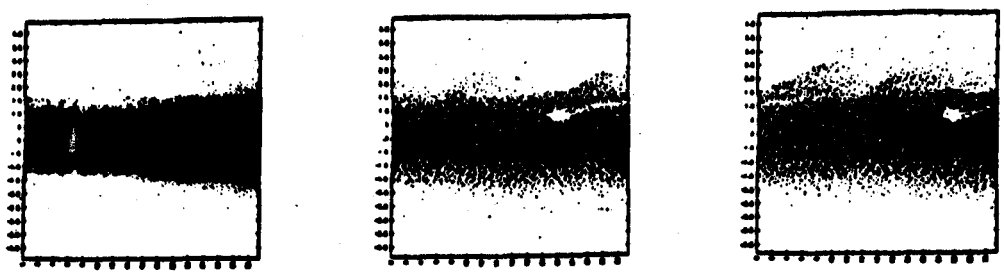

A B C

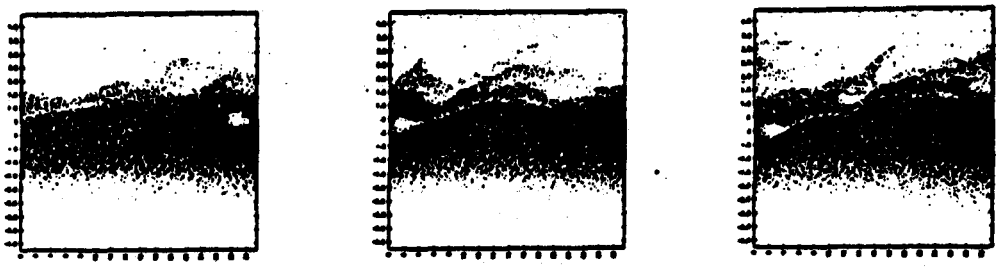

D E F

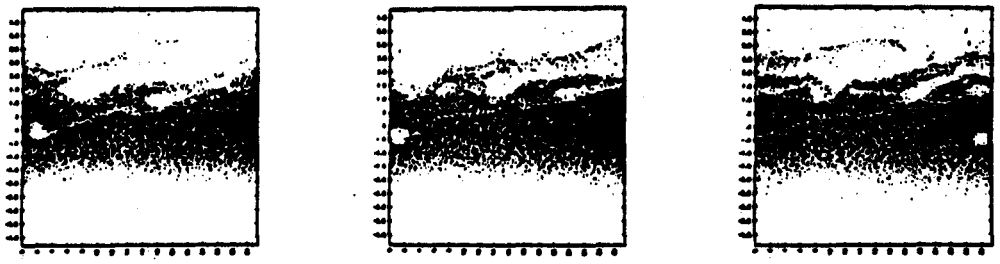

G H

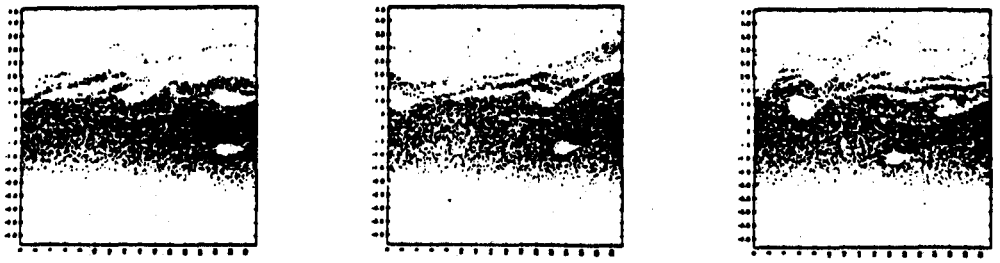

J K L

FIGURE 8

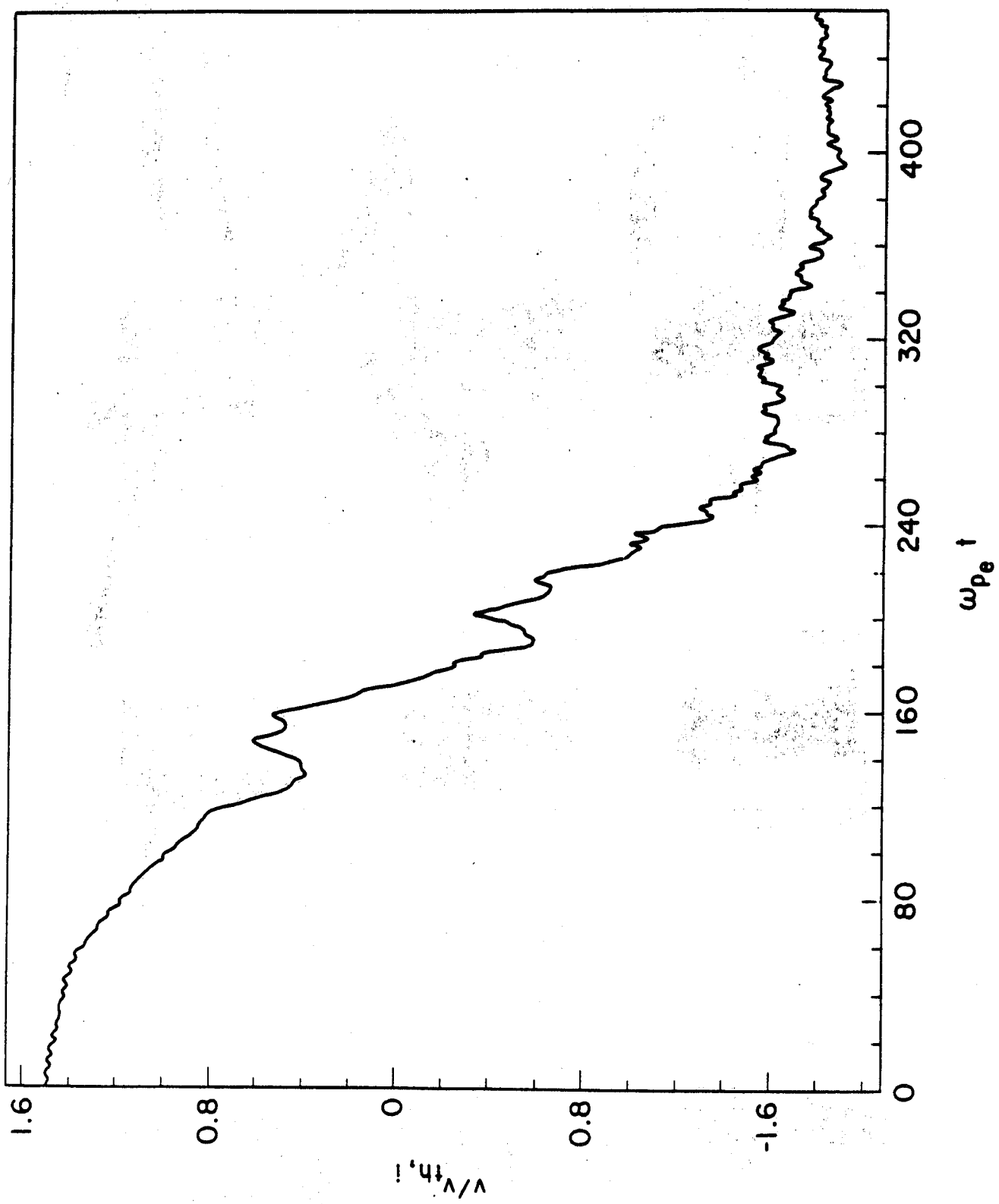

FIGURE 9

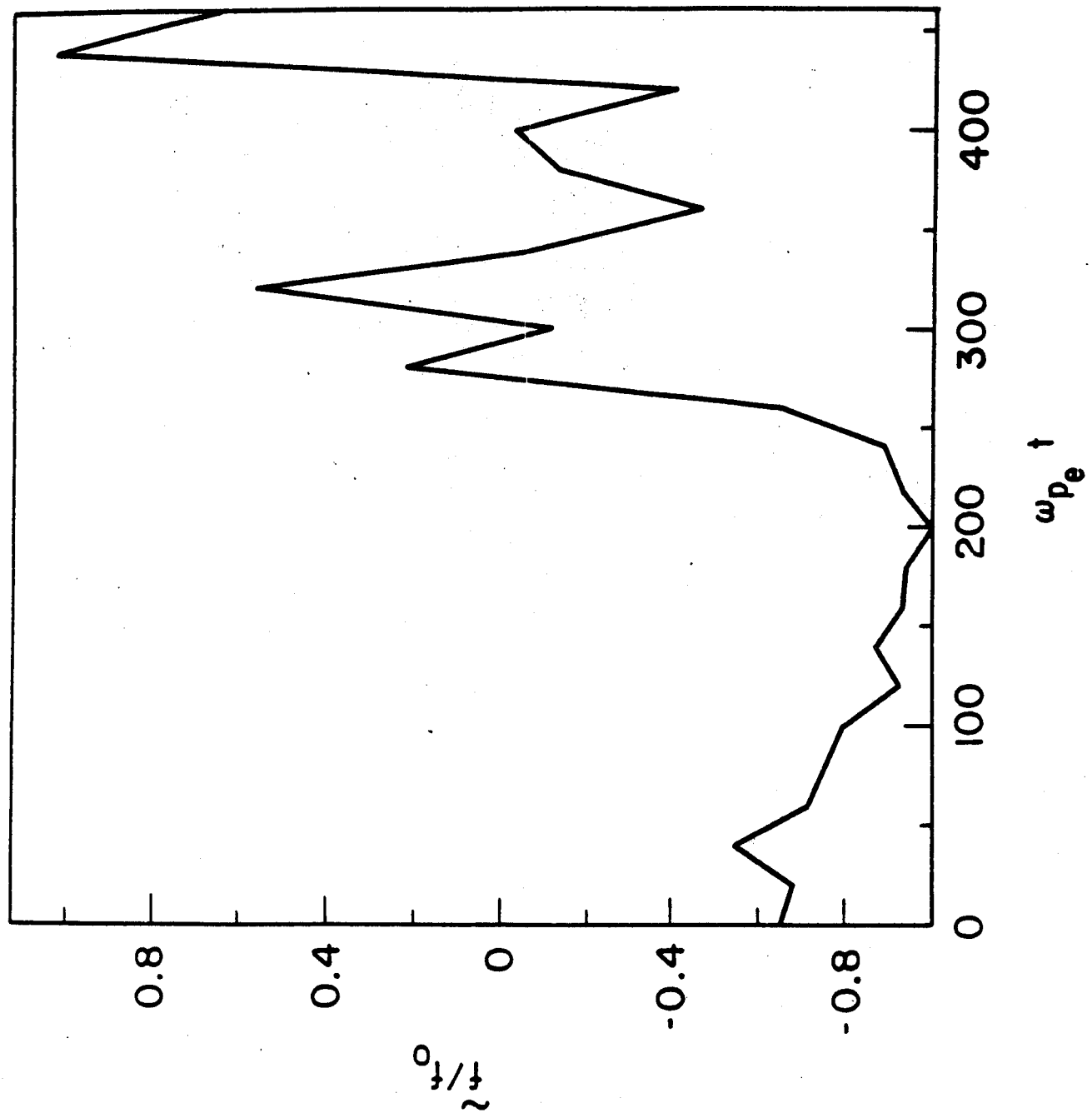

Figure 10

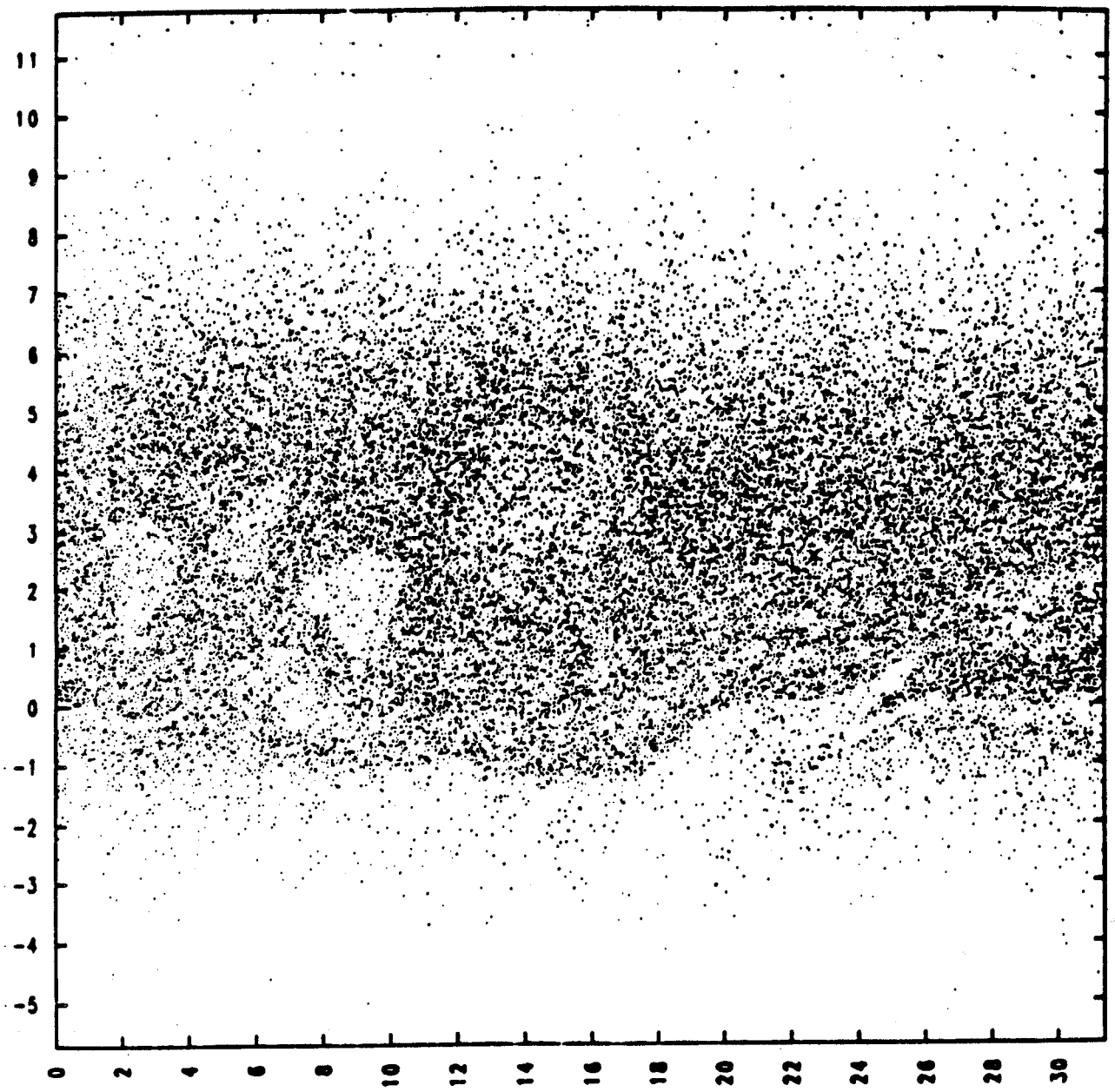

FIGURE 11

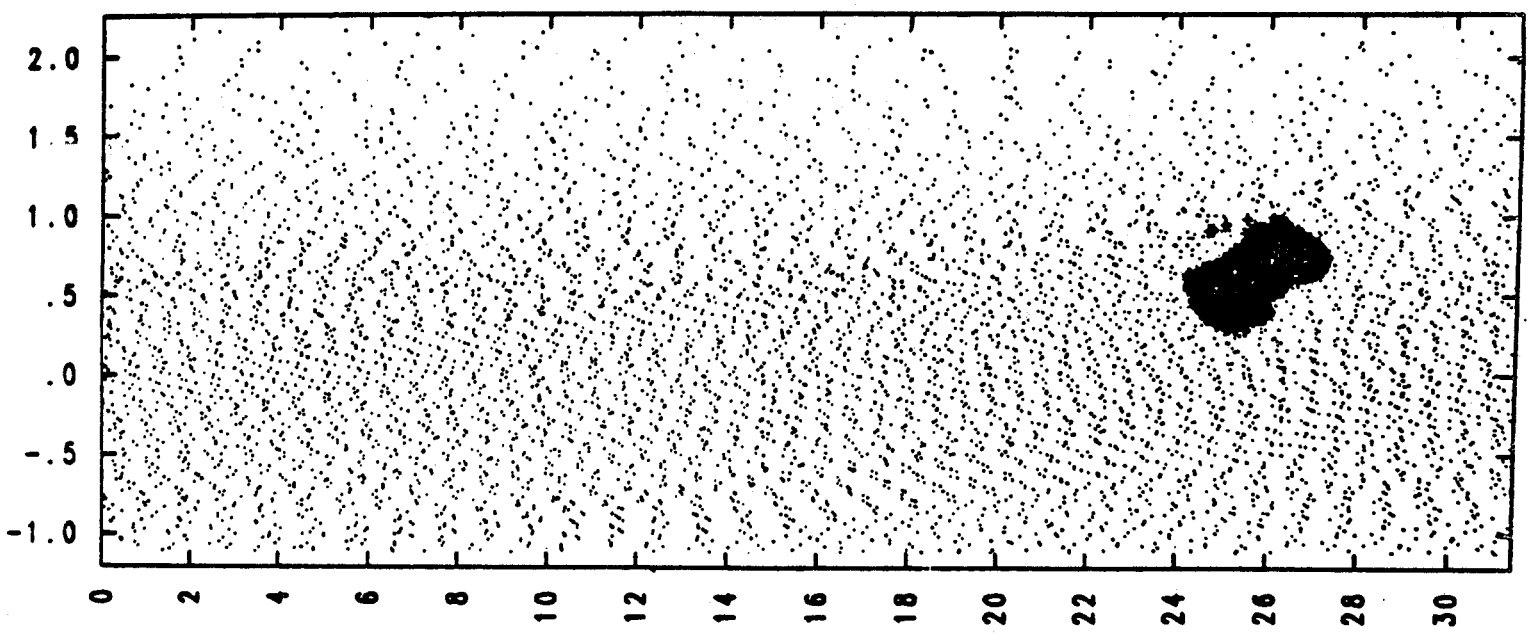

FIGURE 12

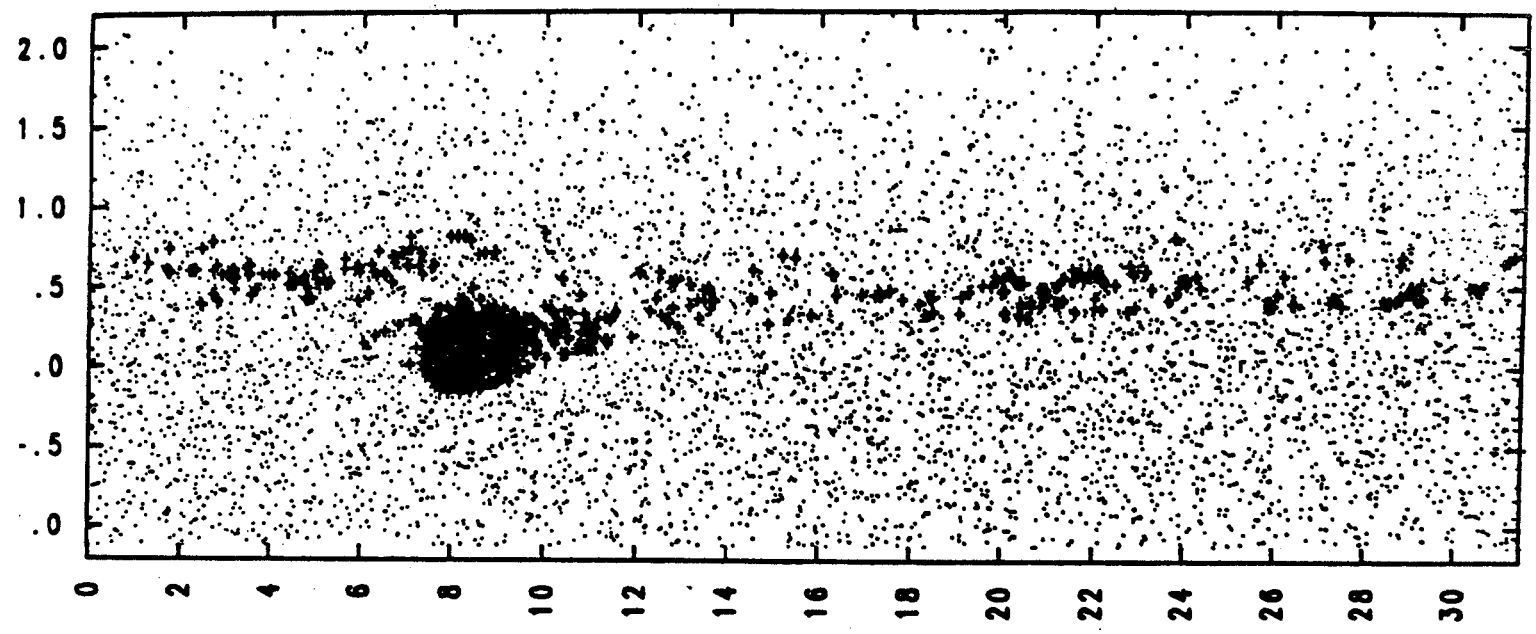

FIGURE 12 (continued)

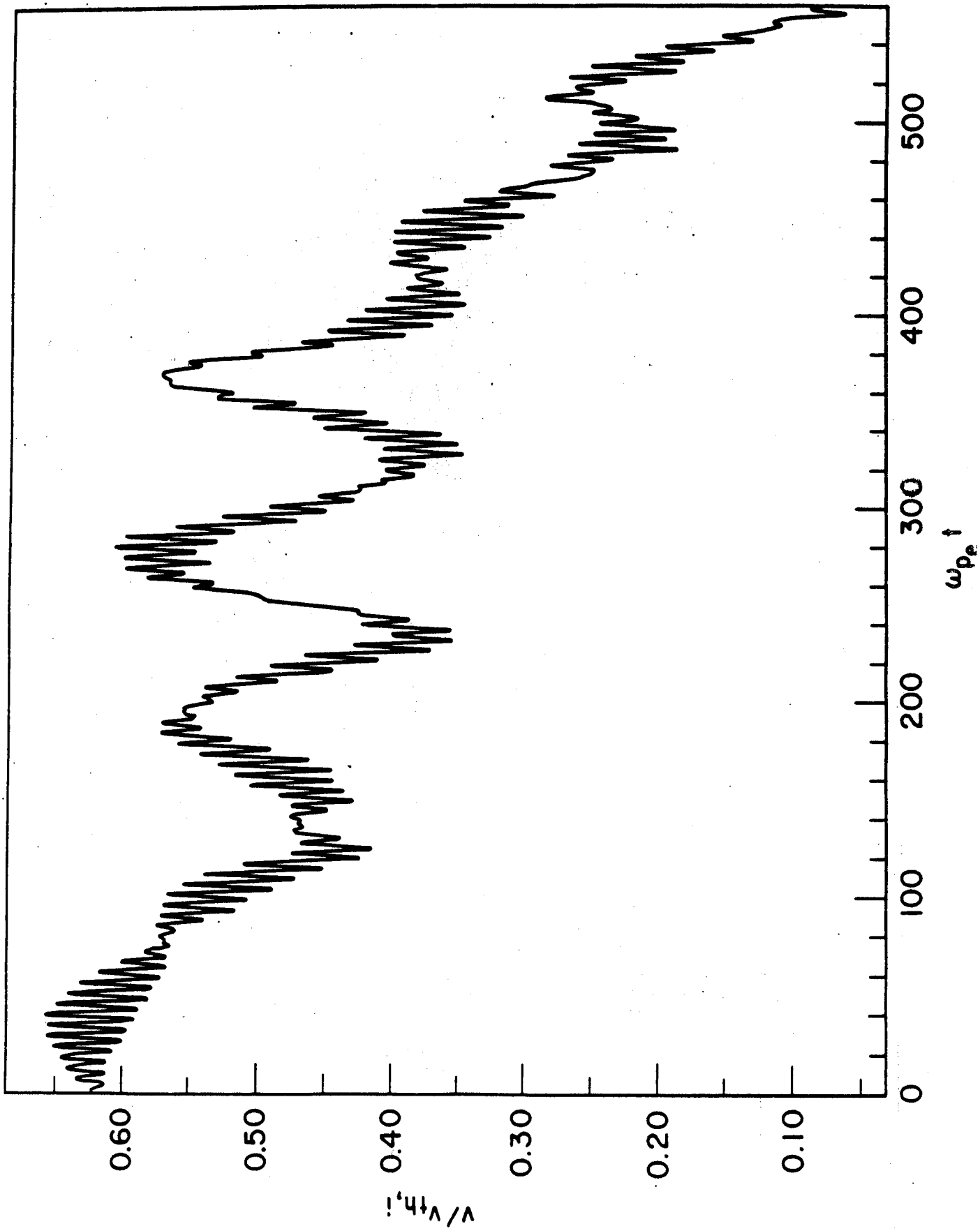

FIGURE 13

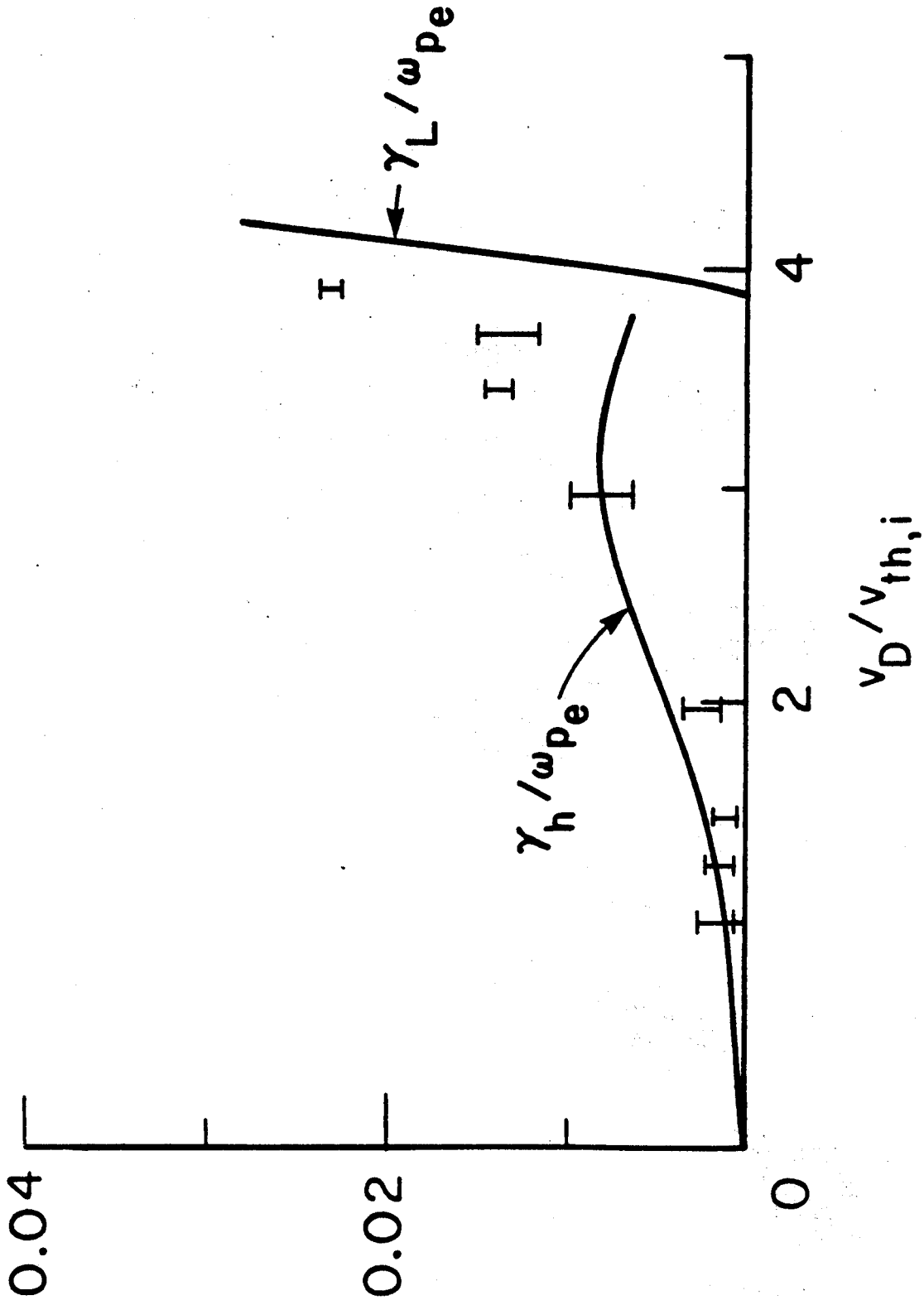

FIGURE 14

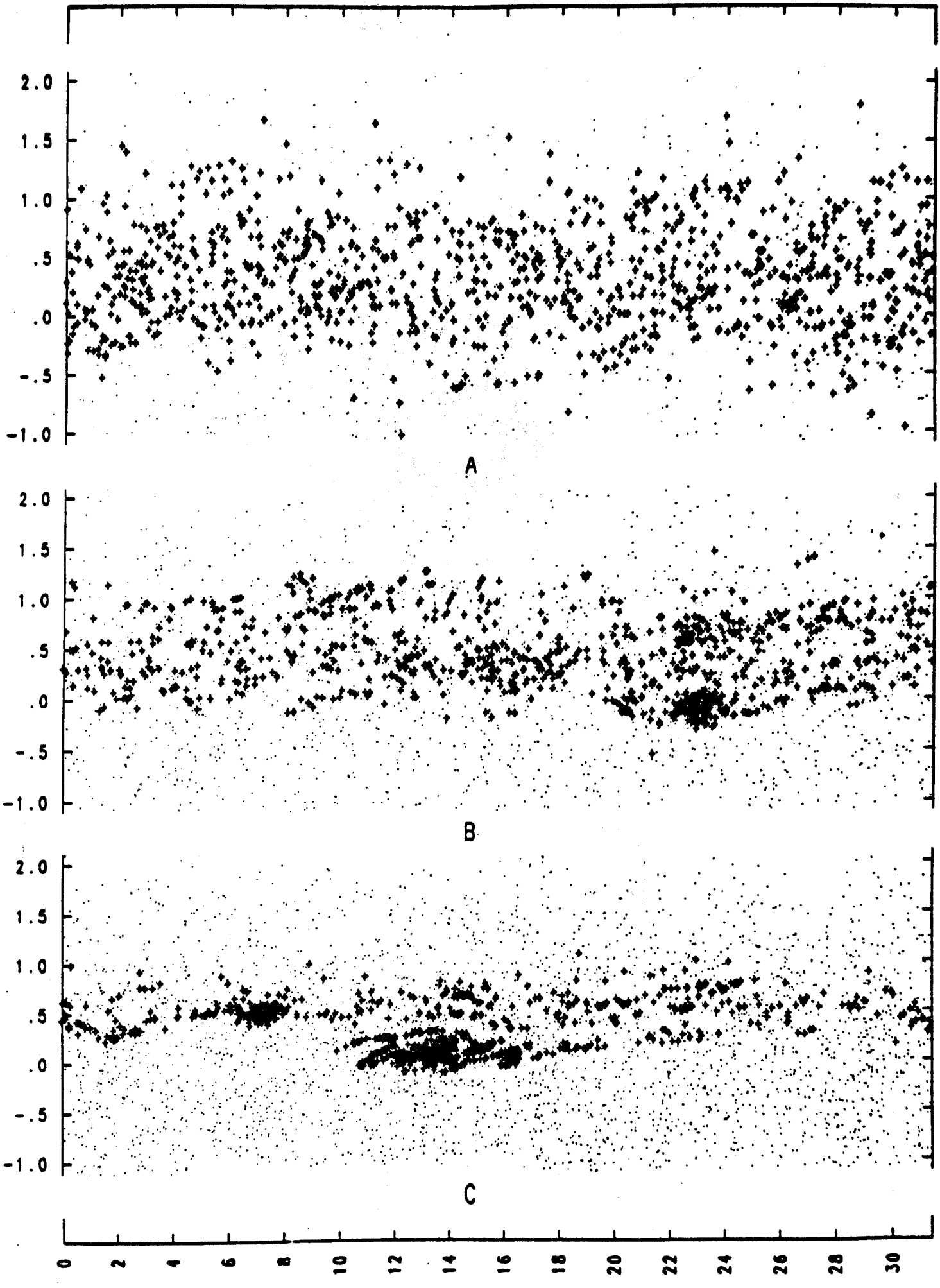
2.0
1.5
1.0
.5
.0
-.5
-1.0
A
2.0
1.5
1.0
.5
.0
-.5
-1.0
B
2.0
1.5
1.0
.5
.0
-.5
-1.0
C
0
2
4
6
8
10
12
14
16
18
20
22
24
26
28
30

FIGURE 15

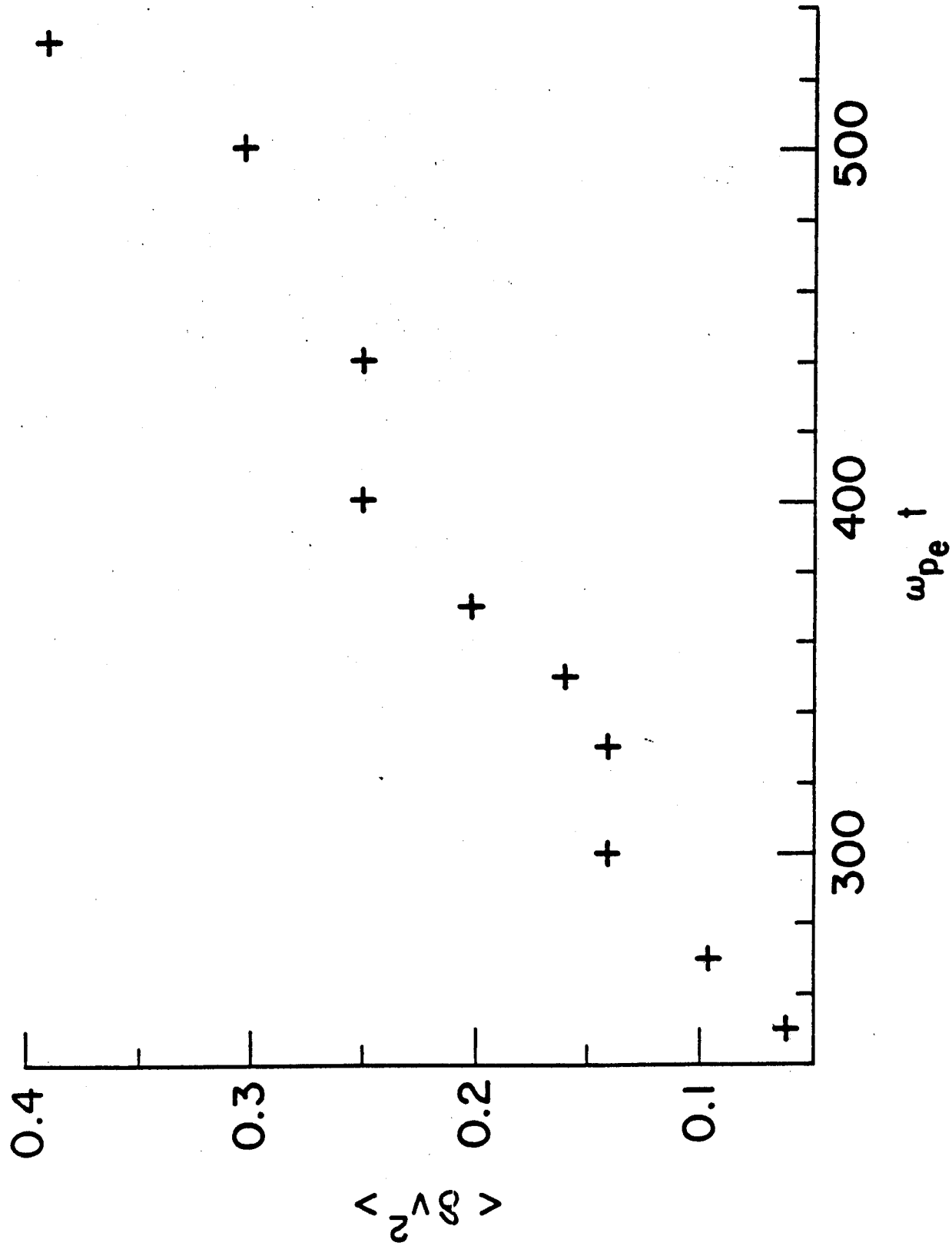

FIGURE 16

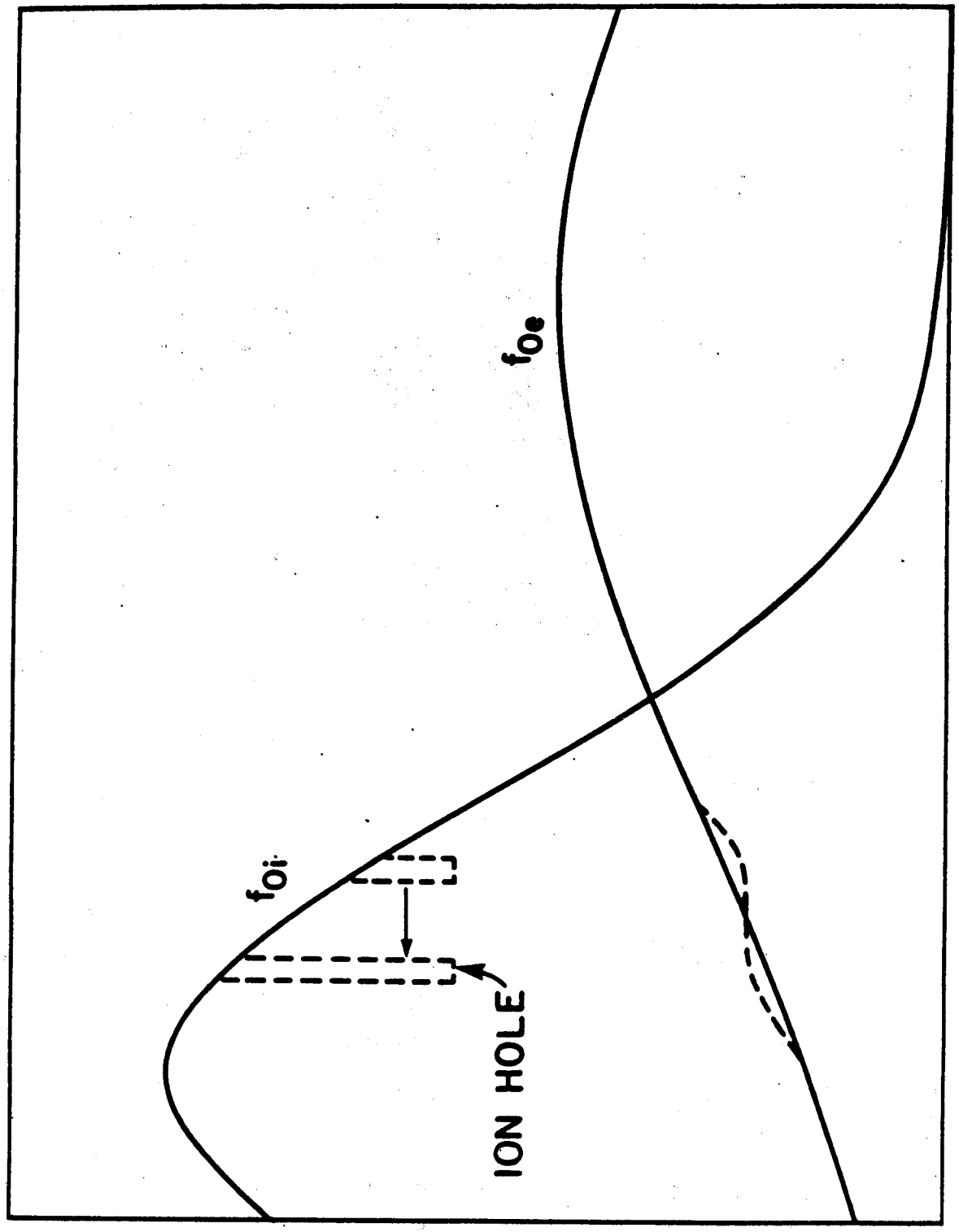

FIGURE 17

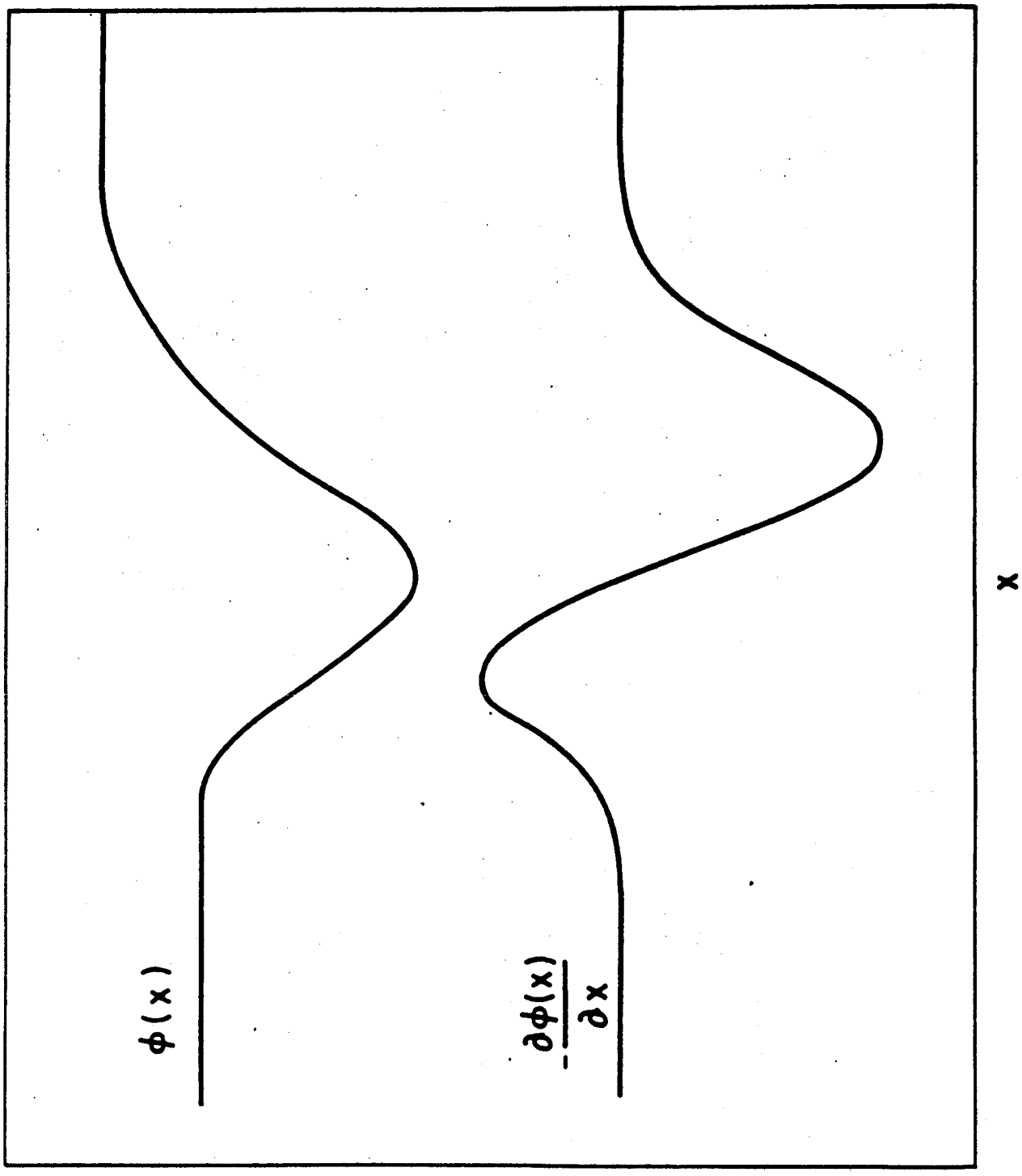

FIGURE 18

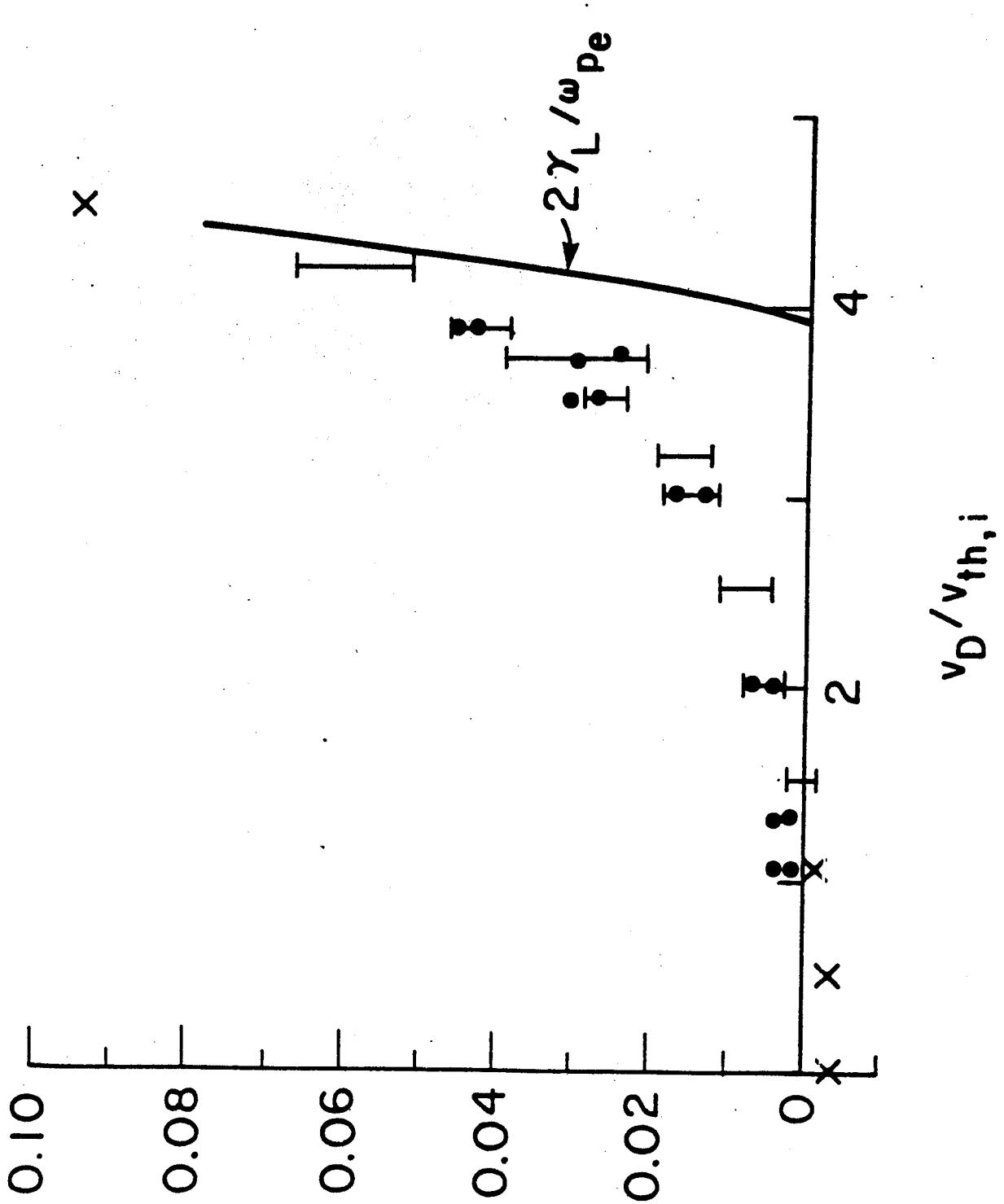

FIGURE 19